

# Exciton scattering model of carrier multiplication in semiconductor nanocrystals

Andrei Piryatinski\* and Kirill A. Velizhanin

Center for Nonlinear Studies (CNLS), Theoretical Division,  
Los Alamos National Laboratory, Los Alamos, NM 87545

(Dated: July 22, 2022)

Effect of carrier multiplication (CM) in semiconductor nanocrystals is systematically treated by employing the exciton scattering approach. By using projection operators, we reduce Coulomb coupled multi-exciton dynamics to the scattering dynamics in the space spanning single- and bi-exciton states, and derive a closed set of equations determining the scattering matrix elements. This allows us to interpret CM dynamics as a series of odd-order interband scattering events. Further using the time-dependent density matrix formalism, we provide rigorous description of CM dynamics induced by finite-time pump pulse. Within this approach both processes of single- and bi-exciton photo-generation and following population relaxation are treated on the same footing. This constructs a framework for numerical calculations and comparison of the quantum efficiencies associated with each process. Important for applications, limit of weak interband Coulomb coupling is considered. Finally, we demonstrate that previously used theoretical models can be recovered from the proposed one as limiting cases.

PACS numbers: 71.10.-w, 71.35.-y, 72.40.+w, 73.21.La, 78.67.Hc, 82.53.Mj

## I. INTRODUCTION

Carrier multiplication (CM) in semiconductor materials is a process of more than one electron-hole pair generation per single absorbed photon. We consider a general case when high energy electron-hole pairs can consist of free carriers as typically considered in bulk or can be confined exciton states formed in nanocrystals (NCs). CM is naturally characterized by Quantum Efficiency (QE) which is a number of electron-hole pairs generated per absorbed photon, and by the activation energy threshold (AET) below which the effect becomes negligible. Extensive studies of this effect are motivated by potential applications in photovoltaic, photoelectrochemical, and energy storage devices.<sup>1,2,3,4,5,6,7</sup>

CM was first investigated in bulk materials using photocurrent measurements,<sup>8,9,10,11,12</sup> and recently revisited using terahertz time-domain spectroscopy.<sup>13</sup> Theory of CM in bulk treats this effect as a sequence of primary photoexcitation event when a *single* electron-hole pair is created by a photon, and secondary process of the electron and hole population relaxation during which CM occurs.<sup>14,15,16,17</sup> The population relaxation dynamics represents a competition between impact ionization process when excess kinetic energy of hot electron/hole is transferred to create another electron-hole pair<sup>15,18,19</sup> and the process of phonon-assisted relaxation conserving total number of carriers and resulting in their cooling.<sup>16,17</sup>

In bulk, strict energy along with quasi-momentum conservation constraints determine AET<sup>20,21</sup> and spectral dependence of QE as a function of photon energy<sup>16</sup>. For a variety of semiconductor materials, it was found that the *lower boundary* for AET is about  $3E_g$  where  $E_g$  is the bulk band gap energy.<sup>20,21</sup> However, the photocurrent<sup>8,9,10,11,12</sup> and optical<sup>13</sup> measurements showed that the AET for most considered materials is

$$\gtrsim 4E_g^{8,9,10,11,12}$$

In semiconductor NCs, it is expected that quantum confinement related relaxation of quasi-momentum conservation constraint<sup>22</sup>, decrease in the phonon-relaxation rate<sup>23</sup>, and enhancement of Coulomb interaction between the carriers<sup>22,24</sup> should lead to the increase in QE and lowering AET. Efficient CM has been reported in colloidal NCs using time-resolved transient absorption (pump-probe) and time-resolved photoluminescence techniques.<sup>25,26,27,28,29,30,31,32,33,34,35</sup> Reported values of AET vary in the range of  $2 - 3E_g$  with  $E_g$  denoting NC's band gap energy. It has been further speculated by using the bulk-type model with relaxed quasi-momentum conservation rule that depending on the ratio of electron and hole effective masses the AET can reach minimum value of  $2E_g$  determined by the energy conservation constraint.<sup>28</sup>

These experimental results have been challenged by a number of reports claiming significantly lower QE or even the absence of the CM effect.<sup>36,37,38</sup> CM has been further reconfirmed, however, with observed values of QE varying in a broad range starting below QE in bulk materials.<sup>39,40,41,42</sup> The variation of QE could possibly rise from experimental inaccuracy,<sup>37,43</sup> sample-to-sample variation in surface preparation,<sup>44,45</sup> and contribution from extraneous effects such as photocharging<sup>39</sup>. These issues rise an important question: What are specific quantum confinement induced features that distinguish CM in NCs from bulk semiconductors?<sup>41</sup> Addressing this question requires theoretical insight into the investigated phenomena. Currently, there are three approaches outlined below that propose different scenarios of CM in NCs.

*Coherent Superposition Model* of resonant (almost degenerate) single- and bi-exciton states implementing the density matrix formalism has been proposed by Shabaev, Efros, and Nozik.<sup>46</sup> In contrast to the bulk materials,

this model states that the primary event of single photon absorption leads to the preparation of coherent superposition (oscillations) between the single- and bi-exciton states that are almost degenerate. Secondary process of phonon-induced intraband relaxation just stabilizes the populations leading to efficient bi-exciton production due to the fast bi-exciton intraband relaxation rate. No experimental observations of the oscillations have been reported yet. Enhancement of the QE using this model requires strong Coulomb interaction between single- and bi-exciton states which has not been confirmed experimentally. The model also disregards the effect of the single-/bi-exciton density of states (DOS) by considering only one single-exciton and one bi-exciton states coupled through Coulomb interaction.

Assuming weak Coulomb coupling between single- and bi-exciton states and long compared to the dephasing time scale optical pump pulse, QE can be evaluated from the Fermi's Golden Rule.<sup>27,47</sup> This approach referred as *Direct Photogeneration Model* model, predicts the following two pathways for direct bi-exciton production during the primary photon absorption event. First pathway introduced by Schaller, Agranovich and Klimov described resonant bi-exciton generation via virtual single-exciton states.<sup>27</sup> The other pathway considered by Rupasov and Klimov accounts for non-vanishing Coulomb matrix elements between exciton vacuum (filled valence band) and bi-exciton states. This coupling leads to the stabilization of bi-exciton populations through resonant intraband optical transitions.<sup>47</sup> The authors estimate contributions of both pathways and claim that they become efficient in NCs since the quasi-momentum conservation constraint is relaxed. As a result, the enhancement of QE comes from high bi-exciton DOS. Independent quantum chemistry calculations confirm a possibility of direct carrier photogeneration in semiconductor clusters.<sup>48</sup> The drawback of Direct Photogeneration Model is that no secondary events of population relaxation on QE is considered.

A number of reported calculations suggest that in contrast to the mechanisms outlined above and similar to the bulk materials, CM in NCs occurs solely due to the competing phonon-assisted relaxation and impact ionization processes that follow primary single-exciton photoexcitation event. We will refer to this approach as *Impact Ionization Model* model through out this paper. Specifically, Franceschetti, An, and Zunger considered the spectral dependence of impact ionization rate and Auger recombination (the process inverse to the latter one) rate using the atomistic pseudopotential calculations.<sup>49</sup> Allan and Delerue used tight-binding model to simulate competing processes of impact ionization and phonon-assisted relaxation.<sup>50</sup> Analysis based on these models emphasizes the importance of high ratio of bi- to single-exciton DOS for efficient CM.

Further development of this approach led to DOS based comparison of QE due to impact ionization and direct photogeneration,<sup>51</sup> evaluation of the band-structure

effects on QE in a variety of NC materials,<sup>52</sup> and modeling the influence of surface defects on QE.<sup>53</sup> Interestingly, Rabani and Baer argued the importance of the trion DOS (in contrast to the bi-exciton DOS) directly entering the impact ionization and Auger recombination rates where strict selection rules enter through the Coulomb matrix elements.<sup>54</sup>

Currently, Coherent Superposition Model, Direct Photogeneration Model, and Impact Ionization Model are considered as alternative approaches whose application range is debated. In this paper, we present general *Exciton Scattering Model*, and demonstrate that perviously proposed models are fundamentally connected and represent limiting cases of the proposed Exciton Scattering Model. The paper is organized as follows, in Sec. II, projection operator technique is employed to reduce coupled multi-exciton dynamics to single- and bi-exciton scattering dynamics in Hilbert space, and further derive a closed set of equations for the interband scattering matrix. In Sec. III, we use density matrix formalism combined with adopted exciton scattering approach to obtain general expressions for QE that naturally describe primary event of single- and bi-exciton photogeneration due to *finite* pump pulse and population relaxation dynamics. Important for applications, limiting case of weak Coulomb coupling is introduced in Sec. IV where a closed set of equations for limiting QE is presented. In Sec. V, we discuss connections of Exciton Scattering Model with previously proposed models and conclude.

## II. MULTI-EXCITON DYNAMICS IN HILBERT SPACE

In this section, we begin our analysis by introducing the many-body electronic Hamiltonian in the multi-exciton representation which accounts for the contributions of all the Coulomb terms. The latter can be partitioned into the terms that conserve total number of excitons and determine their binding energies, and the terms that do not conserve number of excitons giving rise to the CM dynamics. Exact treatment of the dynamics in the total multi-exciton space is not feasible, and, therefore, we restrict the dynamics to the reduced space spanning the single- and bi-exciton states by using the projection operator technique. This approach allows us to account for the effect of higher-multiplicity (tri-, four-, *etc.*) exciton states on the dynamics in the reduced space, and to formulate conditions allowing one to neglect the latter effect. Since the projected dynamics is restricted to coupled single- and bi-exciton manifolds only, they can be treated by performing exact summation of perturbation series, where the *odd-order* interband scattering events describe CM dynamics.

### A. The multi-exciton Hamiltonian

Let us consider valence and conduction bands of a semiconductor NC where single electron and hole states are known within the Hartree-Fock approximation or equivalently within the effective mass envelope function formalism. This leads to the many-body electronic Hamiltonian  $\hat{\mathcal{H}}$  accounting for these non-interacting single particle states, and all possible Coulomb interactions between them.<sup>55</sup> An explicit form of the Hamiltonian is given in Appendix A. Not all the Coulomb interaction terms in  $\hat{\mathcal{H}}$  conserve the total number of electrons and holes, although, the Hamiltonian conserves total charge. Therefore, electrically neutral electron-hole pair (excitons) dynamics is uncoupled from the charged states dynamics. This allows us to focus on the former dynamics determined by the multi-exciton Hamiltonian

$$\hat{H}_{MX} = \hat{H}_{MX}^{(0)} + \hat{H}_{MX}^{(1)} + \hat{H}_{MX}^{(2)}, \quad (1)$$

whose derivation is provided in Appendix A.

The block-matrix representation of the multi-exciton Hamiltonian is shown in Fig 1, where the  $\langle 0|\hat{\mathcal{H}}|0\rangle$ -block denotes the exciton vacuum, i.e. filled valence band, whose energy is set to zero. The other diagonal (red) blocks describe single-exciton, bi-exciton, *etc.*, subspaces. These terms read

$$\hat{H}_{MX}^{(0)} = \sum_{\bar{n} \geq 1} \sum_{p \geq 1} |x_p^{\bar{n}}\rangle \hbar\omega_p^{\bar{n}} \langle x_p^{\bar{n}}|, \quad (2)$$

where  $|x_p^{\bar{n}}\rangle$  is the  $p$ -th exciton states with multiplicity  $\bar{n}$  characterized by the energy  $\hbar\omega_p^{\bar{n}}$ . This energy already includes the  $\bar{n}$ -particle binding interactions which can be calculated, e.g. by the block-wise matrix diagonalization.

The off-diagonal Coulomb interaction (green and blue) blocks do not conserve the total number of electrons and holes resulting from the coupling between the exciton states with different multiplicity. Green off-diagonal blocks describe the processes changing multiplicity by one, and blue off-diagonal blocks by two. Note that the bi-exciton states are coupled to the vacuum, whereas the single-exciton states are uncoupled from the vacuum. This is a result of the Hartree-Fock representation eliminating the latter interactions. General expression for the off-diagonal terms in the multi-exciton Hamiltonian is

$$\hat{H}_{MX}^{(\bar{i})} = \sum_{\bar{n}} \sum_{pq} |x_p^{\bar{n}}\rangle V_{p,q}^{\bar{n},\bar{n}+\bar{i}} \langle x_q^{\bar{n}+\bar{i}}| + h.c., \quad (3)$$

where  $V_{p,q}^{\bar{n},\bar{n}+\bar{i}} = \langle x_p^{\bar{n}}|\hat{\mathcal{H}}|x_q^{\bar{n}+\bar{i}}\rangle$  is the interband multi-exciton interaction matrix element with  $\bar{i} = 1, 2$  describing the multiplicity variation.

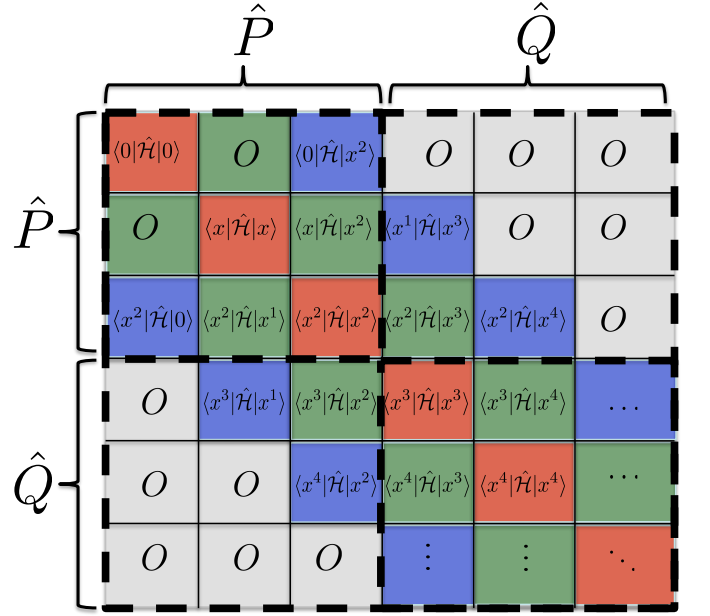


FIG. 1: The multi-exciton Hamiltonian in the block-matrix representation. The  $\langle 0|\hat{\mathcal{H}}|0\rangle$ -block is the exciton vacuum, and the rest of the diagonal (red) blocks represent the Hamiltonian components in the single-exciton, bi-exciton, *etc.* subspaces. Green off-diagonal blocks describe Coulomb interactions between the latter components changing exciton multiplicity by one, and the blue blocks by two. 0-blocks mean zero-matrices. Four quadrants marked by the black dash describe the partitioning of the multi-exciton Hamiltonian by the projection operators  $\hat{P}$  and  $\hat{Q}$ . The upper left quadrant is the projected Hamiltonian Eqs. (6) – (8) acting in the space spanning the single- and bi-exciton states.

### B. Projected dynamics in single- and bi-exciton space

Dynamics in the total multi-exciton Hilbert space is fully defined by the propagator

$$\hat{U}(t) = \Theta(t) \exp \left[ -i\hbar^{-1} \hat{H}_{MX} t \right], \quad (4)$$

whose calculation and general analysis is not feasible due to the highly growing number of multi-exciton states. Thus, we introduce a convenient representation allowing for approximate calculations of this propagator.

The CM processes excited near AET result in photo-generation of single- and bi-exciton states only. On the other hand, the higher-multiplicity exciton states can still affect their dynamics. Therefore, we consider projected dynamics within the space spanned by the single- and bi-exciton states, and seek the conditions allowing us to neglect the effects associated with the higher-multiplicity states. This can be naturally done by introducing the following projection operator onto the space of single- and bi-exciton states

$$\hat{P} = \sum_{a \geq 0} |x_a\rangle \langle x_a| + \sum_{k \geq 1} |xx_k\rangle \langle xx_k|, \quad (5)$$

and the complementary projection operator  $\hat{Q} = \hat{I} - \hat{P}$  onto the rest of the multi-exciton space.  $\hat{I}$  denotes the unit operator in the total multi-exciton space. To distinguish the single- and bi-exciton states from the higher-multiplicity states  $|x_p^{\bar{n}}\rangle$  where  $n \geq 3$ , we have introduced their new notations such as  $|x_a\rangle$  and  $|xx_k\rangle$ , respectively, and use  $|x_0\rangle$  to denote the exciton vacuum. These notations will be used through out this paper.

The partitioning of the multi-exciton Hamiltonian by the projection operators  $\hat{P}$  and  $\hat{Q}$  is illustrated in Fig. 1, where the *projected* Hamiltonian  $\hat{H} = \hat{P}\hat{H}_{MX}\hat{P}$  is a sum of two terms

$$\hat{H} = \hat{H}_0 + \hat{V}_C. \quad (6)$$

Here, the first term

$$\hat{H}_0 = \sum_{a \geq 1} |x_a\rangle \hbar \omega_a^x \langle x_a| + \sum_{k \geq 1} |xx_k\rangle \hbar \omega_k^{xx} \langle xx_k|, \quad (7)$$

describes non-interacting single- and bi-exciton states, and the second one

$$\hat{V}_C = \sum_{a \geq 0} \sum_{k \geq 1} |x_a\rangle V_{a,k}^{x,xx} \langle xx_k| + h.c., \quad (8)$$

represents the interband Coulomb interactions  $V_{a,k}^{x,xx}$  between the states, as well as the vacuum to bi-exciton couplings  $V_{k,0}^{xx,x}$ . Explicit representations for interaction matrix elements in terms of single-particle couplings, and related matrix equations defining the single- and bi-exciton states are provided in Appendix A.

The dynamics restricted to the subspace of interest is fully defined by the projected propagator  $\hat{G}(t) = \hat{P}\hat{U}(t)\hat{P}$  whose representation in the frequency (Fourier) domain is<sup>56</sup>

$$\hat{G}(\omega) = i \left[ \omega - \hat{h}_{eff}(\omega) + i\gamma \right]^{-1}, \quad (9)$$

where  $\gamma$  denotes finite broadening associated with the exciton-phonon coupling. The non-local effective Hamiltonian entering this Green function can be partitioned into the sum of the diagonal and off-diagonal terms

$$\hat{h}_{eff}(\omega) = \hat{h}(\omega) + \hat{v}(\omega), \quad (10)$$

which have the following form

$$\hat{h}(\omega) = \hbar^{-1} \hat{H}_0 + \hat{k}_d(\omega), \quad (11)$$

$$\hat{v}(\omega) = \hbar^{-1} \hat{V}_C + \hat{k}_o(\omega), \quad (12)$$

respectively. The first terms in Eqs. (11) and (12) are components of the projected Hamiltonian  $\hbar^{-1}\hat{H}$  (Eq. (6)–(8)) describing the propagation of the coupled single- and bi-exciton states. The second terms, accounting for the effect of the higher-multiplicity exciton states, are diagonal  $\hat{k}_d(\omega)$  and off-diagonal  $\hat{k}_o(\omega)$  components of the non-local memory kernel, respectively.

The memory kernel components can be explicitly represented in the multi-exciton bases as

$$\hat{k}_d(\omega) = \hbar^{-2} \sum_{\bar{n}\bar{m} \geq 3} \sum_{pq \geq 1} \left[ \sum_{ab \geq 0} |x_a\rangle V_{a,p}^{x,\bar{n}} \tilde{G}_{p,q}^{\bar{n},\bar{m}}(\omega) V_{q,b}^{\bar{m},x} \langle x_b| \right. \quad (13)$$

$$\left. + \sum_{kl \geq 1} |xx_k\rangle V_{k,p}^{xx,\bar{n}} \tilde{G}_{p,q}^{\bar{n},\bar{m}}(\omega) V_{q,l}^{\bar{m},xx} \langle xx_l| \right],$$

$$\hat{k}_o(\omega) = \hbar^{-2} \sum_{\bar{n}\bar{m} \geq 3} \sum_{pq \geq 1} \sum_{a \geq 0} \sum_{k \geq 1} \left[ |x_a\rangle V_{a,p}^{x,\bar{n}} \tilde{G}_{p,q}^{\bar{n},\bar{m}}(\omega) V_{q,l}^{\bar{m},xx} \langle xx_l| \right. \quad (14)$$

$$\left. + |xx_l\rangle V_{l,q}^{xx,\bar{m}} \tilde{G}_{q,p}^{\bar{m},\bar{n}}(\omega) V_{p,a}^{\bar{n},x} \langle x_a| \right],$$

where  $V_{a,p}^{x,\bar{n}}$  ( $V_{l,q}^{xx,\bar{m}}$ ) denotes the interaction matrix elements (Eq. (3)) which couple single-exciton (bi-exciton) states with the higher-multiplicity, i.e.  $\bar{n}\bar{m} \geq 3$ , states. The matrix elements  $\tilde{G}_{p,q}^{\bar{n},\bar{m}}(\omega) = \langle x_p^{\bar{n}} | \tilde{G}(\omega) | x_q^{\bar{m}} \rangle$  of the propagator

$$\tilde{G}(\omega) = i \left[ \omega - \hbar^{-1} \hat{Q} \hat{H}_{MX} \hat{Q} \right]^{-1}, \quad (15)$$

describe the projected dynamics in the higher-multiplicity exciton space defined by  $\hat{Q}$  (the lower right quadrant in Fig 1).

The use of the projection operators has allowed us to map the propagator acting in the multi-exciton space (Eq. (4)) to the projected propagator acting in the space of single- and bi-exciton states (Eqs. (9)–(15)). This representation is exact, since the effect of the higher-multiplicity exciton states is fully accounted for through the memory kernel (Eqs. (13) and (14)). The dynamics of interest can now be interpreted as the uncoupled propagation within single- and bi-exciton manifolds described by the following zeroth-order Green function

$$\hat{g}(\omega) = i \left[ \omega - \hat{h}(\omega) + i\gamma \right]^{-1}, \quad (16)$$

and the scattering events between these manifolds induced by the interaction operator  $\hat{v}(\omega)$ .

### C. Single- and bi-exciton scattering model

To apply the scattering matrix formalism, we represent the projected Green function (Eq. (9)) as a  $2 \times 2$  block matrix

$$\hat{G}(\omega) = \begin{pmatrix} \hat{G}^x(\omega) & \hat{G}^{x,xx}(\omega) \\ \hat{G}^{xx,x}(\omega) & \hat{G}^{xx}(\omega) \end{pmatrix}. \quad (17)$$

The time-dependent components given by the Fourier transformation

$$\hat{G}(t) = \int_{-\infty}^{\infty} \frac{d\omega}{2\pi} \hat{G}(\omega) \exp(-i\omega t), \quad (18)$$

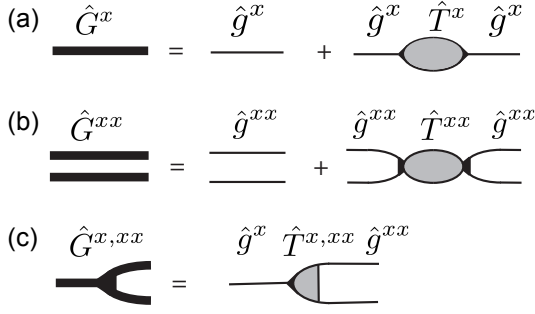


FIG. 2: Feynman diagram representation of the projected propagator  $\hat{G}$  in terms of the scattering operator  $\hat{T}$ . Panels (a) and (b) show the single- and bi-exciton propagator components, respectively. (c) The interband component of the propagator mixing the single- and bi-exciton states.

define the time-evolution of the single- and bi-exciton states as

$$|x_a(t)\rangle = \sum_{b \geq 1} G_{ab}^x(t) |x_b(0)\rangle + \sum_{k \geq 1} G_{a,k}^{x,xx}(t) |xx_k(0)\rangle, \quad (19)$$

$$|xx_k(t)\rangle = \sum_{a \geq 0} G_{k,a}^{x,x}(t) |x_a(0)\rangle + \sum_{l \geq 1} G_{kl}^{xx}(t) |xx_l(0)\rangle. \quad (20)$$

According to Eqs. (19) and (20), the matrix elements  $G_{ab}^x(t)$  and  $G_{kl}^{xx}(t)$  associated with the diagonal blocks in Eq. (17) determine the intraband propagation, and the matrix elements  $G_{a,k}^{x,xx}(t)$  associated with the off-diagonal blocks in Eq. (17) describe the interband scattering processes mixing the single- and bi-exciton states.

Within the scattering matrix formalism, the propagator  $\hat{G}$  satisfies the following matrix equation<sup>57</sup>

$$\hat{G}(\omega) = \hat{g}(\omega) + \hat{g}(\omega) \hat{T}(\omega) \hat{g}(\omega), \quad (21)$$

where  $\hat{g}(\omega)$  is the intraband zeroth-order Green function introduced in Eq. (16). In the adopted block-matrix representation this Green function reads

$$\hat{g}(\omega) = \begin{pmatrix} \hat{g}^x(\omega) & 0 \\ 0 & \hat{g}^{xx}(\omega) \end{pmatrix}. \quad (22)$$

Here, the diagonal blocks  $\hat{g}^x(\omega)$  and  $\hat{g}^{xx}(\omega)$  can be determined numerically using Eq. (16) and matrix inversion procedure. Finally, the scattering operator in the same representation is

$$\hat{T}(\omega) = \begin{pmatrix} \hat{T}^x(\omega) & \hat{T}^{x,xx}(\omega) \\ \hat{T}^{xx,x}(\omega) & \hat{T}^{xx}(\omega) \end{pmatrix}, \quad (23)$$

and contains single-exciton (bi-exciton) components  $\hat{T}^x$  ( $\hat{T}^{xx}$ ), and the interband one  $\hat{T}^{x,xx}$ . The Feynman diagram representation of Eq. (21) is given in Fig. 2. To find solution of Eqs. (21)–(23) we need to know the form of the matrix elements of Eq. (23).

To obtain a closed set of equations for the scattering matrix  $\hat{T}$ , the projected propagator (Eq. (9)) should be

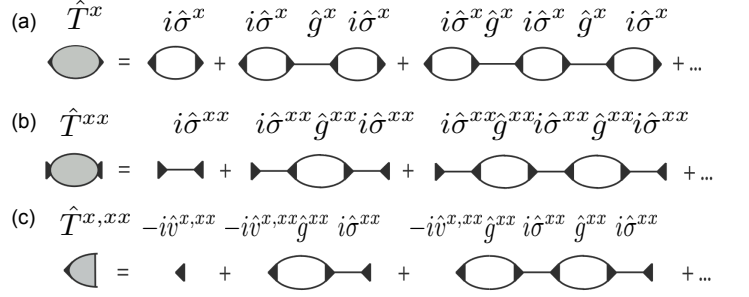


FIG. 3: Feynman diagram expansion for the scattering matrix  $\hat{T}$ . Panels (a) and (b) describe even-order scattering events contributing to the single-exciton and bi-exciton scattering matrix respectively. (c) The odd-order scattering events changing the exciton multiplicity contribute to the interband scattering matrix. The latter processes give rise to CM.

expanded into the power series of the interband coupling operator  $\hat{v}(\omega)$  (Eq. (12)). The expansion terms should be further regrouped to match the form of Eq. (21), where the series between two zeroth-order Green functions can be identified as the scattering operator. Following from this approach, the diagram expansions of the scattering operator are shown in Fig. 3.

Panels (a) and (b), represent the diagrams contributing to the diagonal scattering matrix blocks  $\hat{T}^x(\omega)$  and  $\hat{T}^{xx}(\omega)$ , respectively. Each term there contains *even* number of vertices reflecting even number of interband scattering events. This leads to conservation of the excitons multiplicity, and renormalization of their energies. The summation of the diagram series in panels (a) and (b) results in the common form of linear equations for single-exciton ( $\bar{n} = x$ ) and bi-exciton ( $\bar{n} = xx$ ) scattering matrix elements

$$\sum_{kl} [\delta_{ik} \delta_{lj} - i\sigma_{ik}^{\bar{n}}(\omega) g_{kl}^{\bar{n}}(\omega)] T_{lj}^{\bar{n}}(\omega) = i\sigma_{ij}^{\bar{n}}(\omega). \quad (24)$$

Here, the self-energy matrix elements renormalize bare single- and bi-exciton energies, and according to Fig. 3 (a) and (b) can be represented as

$$\sigma_{ij}^{\bar{n}}(\omega) = i\hbar^{-2} \sum_{kl} v_{i,k}^{\bar{n},\bar{m}}(\omega) g_{kl}^{\bar{m}}(\omega) v_{l,j}^{\bar{m},\bar{n}}(\omega), \quad (25)$$

where  $\bar{m} = xx$  ( $\bar{m} = x$ ) if  $\bar{n} = x$  ( $\bar{n} = xx$ ).

According to Fig. 3 (c), the interband scattering matrix can be determined from the bi-exciton one according to the following expression

$$T_{a,l}^{x,xx}(\omega) = -iv_{a,l}^{x,xx}(\omega) + \sum_{mn} -iv_{a,m}^{x,xx}(\omega) g_{mn}^{xx}(\omega) T_{nl}^{xx}(\omega). \quad (26)$$

This scattering matrix accounts for the *odd*-order scattering events that change the multiplicity of the initial exciton state, and, therefore, describes the CM dynamics.

Equations (21)–(26), derived in this section are exact, since they account for all terms entering the multi-exciton Hamiltonian (Eqs. (1)–(3)). Specifically, these terms determine the single- and bi-exciton binding energies and the interband interactions all affected by the higher-multiplicity exciton states. In terms of the diagrammatic expansions shown in Figs. 2 and 3, this means that single and double lines associated with the components of  $\hat{g}(\omega)$  and the vertices  $\hat{v}(\omega)$  are dressed by these interactions. In practice, however, only approximate representations for  $\hat{g}(\omega)$  and  $\hat{v}(\omega)$  could be found. For instance, the multi-exciton binding energies can be determined approximately or even neglected.

More difficult task is the evaluation of memory kernel entering effective Hamiltonian (Eq. (10)), since the propagator  $\tilde{G}(\omega)$  (Eq. (15)) cannot be calculated exactly. However, we know that the propagator's poles describe the eigenstates (optical resonances) associated with the coupled exciton states of multiplicity three and higher. If these poles are well separated from the single- and bi-exciton resonances participating in the photoexcited dynamics then the memory kernel can be dropped from the projected propagator  $\tilde{G}(\omega)$  (Eq. (9)). This situation is expected to take place in the vicinity of AET depending on the strength of the Coulomb couplings  $V_{a,p}^{x,\bar{n}}$  and  $V_{n,q}^{xx,\bar{m}}$ .

We focus on the photoinduced dynamics in the vicinity of AET, and assume for the *rest* of the paper that the memory kernel effect is negligible. Therefore, the scattering operator can be calculated by solving the set of linear Eqs. (24)–(26) where entering expressions for zeroth-order propagator  $\hat{g}(\omega)$  and interband interaction operator  $\hat{v}(\omega)$  depend on the components of the projected Hamiltonian (Eqs. (6)–(8)), instead of the full effective Hamiltonian (Eqs. (10)–(12)). As a result, the projected propagator (Eqs. (9), (17), and (18)) used below is assumed to depend on the projected Hamiltonian only.

### III. PHOTOINDUCED DYNAMICS IN LIOUVILLE SPACE

We consider carrier dynamics in an ensemble of NCs excited by the pump pulse whose fluence is adjusted so that no more than single photon is absorbed per NC. This results in the creation of either single- or bi-exciton state in each NC absorbing a photon, and the total population is determined through the ensemble average.

The photoinduced ensemble dynamics are illustrated in Fig. 4: Panel (a) shows exciton photogeneration event which occurs on the pump timescale ranging between 50 – 100 fs. During the photogeneration, relative number of single- and bi-exciton states produced by the pump is determined by the interband scattering processes. The photogenerated populations further relax on the timescale of 1 – 10 ps as shown in panel (b). As we demonstrate below, the relaxation includes phonon-assisted cooling to the bottom of single- and bi-exciton

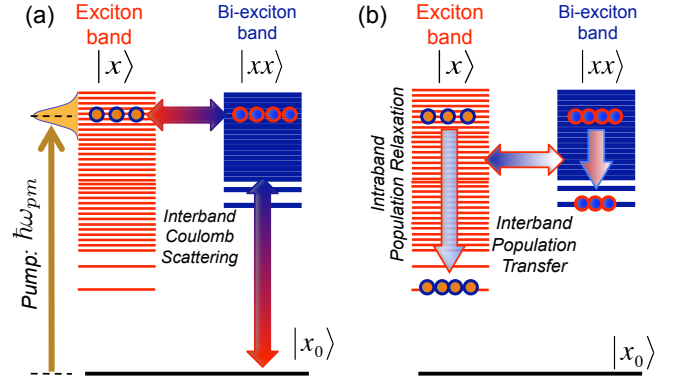


FIG. 4: Level diagram of CM dynamics in an ensemble of NCs. (a) Photoexcitation by pump pulse with central energy  $\hbar\omega_{pm}$  and finite spectral widths results in the generation of single- and bi-exciton populations where the Coulomb scattering mixes all interband and intraband dipole transitions present in Eq. (28). (b) During the population relaxation, both the intraband and the interband processes are mixture of the phonon-assisted processes and Coulomb scattering events.

bands *mixed* with the interband population transfer due to the Coulomb scattering. The population from the bottom of the bi-exciton band finally decays to the lowest single-exciton states through Auger recombination within  $\gtrsim 10$  ps. This process (not shown in Fig. 4) is typically employed for experimental determination of the bi-exciton production yield, and has no contribution to QE. Therefore, we do not consider it in this paper.

To include interaction with the optical pump, we extend the projected Hamiltonian as

$$\hat{H}' = \hat{H} + \hat{V}(t) \quad (27)$$

where the following time-dependent term is added

$$\begin{aligned} \hat{V}(t) = & -E(t) \left[ \sum_{ab \geq 0} |x_a\rangle \mu_{ab}^x \langle x_b| + \sum_{kl \geq 1} |xx_k\rangle \mu_{kl}^{xx} \langle xx_l| \right] \\ & - E(t) \sum_{ak \geq 1} (|x_a\rangle \mu_{ak}^{x,xx} \langle xx_k| + |xx_k\rangle \mu_{ka}^{xx,x} \langle x_a|). \end{aligned} \quad (28)$$

Here, the optical pulse

$$E(t) = \mathcal{E}_{pm}(t) \exp(-i\omega t) + c.c. \quad (29)$$

is characterized by the absolute value of the envelope function  $\mathcal{E}_{pm}(t)$  with the widths  $\tau_{pm}$  describing the pulse duration, and central frequency  $\omega_{pm}$ .<sup>69</sup>

According to Eq. (28), the optical field interacts with all possible transition dipoles which couple the single-exciton states  $\mu_{ab}^x$ , the bi-exciton states  $\mu_{kl}^{xx}$ , and the single- to bi-exciton states  $\mu_{ak}^{x,xx} = \mu_{ka}^{xx,x*}$ . No permanent dipoles are present in the ensemble, i.e.  $\mu_{aa}^x = \mu_{kk}^{xx} = 0$ . In general, all these transitions become allowed due to the Coulomb scattering processes.

Next, we employ the density matrix formalism to include the dissipation processes due to the coupled phonon

bath. Within this formalism, the dynamics of interest are fully described by Liouville equation

$$\dot{\hat{\rho}}(t) = (i\hbar)^{-1} [\hat{H}', \hat{\rho}(t)] + \hat{\mathcal{R}}\hat{\rho}, \quad (30)$$

where the time-dependent density is a  $2 \times 2$  block matrix

$$\hat{\rho}(t) = \begin{pmatrix} \hat{\rho}^x(t) & \hat{\rho}^{x,xx}(t) \\ \hat{\rho}^{xx,x}(t) & \hat{\rho}^{xx}(t) \end{pmatrix}, \quad (31)$$

containing single-exciton  $\hat{\rho}^x(t)$ , bi-exciton  $\hat{\rho}^{xx}(t)$  components, and coherences between single and bi-exciton states  $\hat{\rho}^{xx,x}(t)$ . Specific form of the relaxation term  $\hat{\mathcal{R}}\hat{\rho}$  in Eq. (30) depends on the adopted exciton-phonon interaction model.

### A. Phonon-assisted relaxation model

To describe the phonon-assisted dynamics, we assume that the phonon bath has continuous spectral density, and there is no phonon bottleneck.<sup>58,59,60,61</sup> An explicit form of the spectral density depends on the environment model with adjustable parameters such as spectral width and electron-phonon coupling strength. The simplest model which can be employed in our case is the model of single- and bi-exciton states linearly coupled to the phonon coordinates  $\{q_\alpha\}_{\alpha=1,2,3,\dots}$ . The related Hamiltonian is

$$\hat{H}_{ep} = \hat{H}_i + H_p, \quad (32)$$

where the exciton-phonon interaction term

$$\begin{aligned} \hat{H}_i = & \sum_{ab;\alpha} |x_a\rangle Y_{ab;\alpha}^x q_\alpha \langle x_b| + \sum_{kl;\alpha} |xx_k\rangle Y_{kl;\alpha}^{xx} q_\alpha \langle xx_l| \\ & + \sum_{ak;\alpha} \left( |x_a\rangle Y_{ak;\alpha}^{x,xx} q_\alpha \langle xx_k| + |xx_k\rangle Y_{ka;\alpha}^{xx,x} q_\alpha \langle x_a| \right), \end{aligned} \quad (33)$$

contains the intraband single-exciton (bi-exciton) coupling matrix elements  $Y_{ab;\alpha}^x$  ( $Y_{ab;\alpha}^{xx}$ ) to  $\alpha$ -th phonon mode, and the interband coupling matrix elements  $Y_{ka;\alpha}^{xx,x}$ . The connection between the former quantities and the *electron*-phonon coupling constants from the many-body Hamiltonian is given in Appendix B. The second term in Eq. (32) is the uncoupled phonon Hamiltonian whose form depends on specific environment model.

Assuming weak exciton-phonon coupling, we follow a standard projection operator method to eliminate the bath degrees of freedom resulting in Markov approximation for  $\hat{\mathcal{R}}\hat{\rho}$ .<sup>62,63</sup> The basis set in which equilibrium (Gibbs) distribution  $\bar{\rho}$  can be recovered as zero eigenvalue of the relaxation operator, i.e.  $\hat{\mathcal{R}}\bar{\rho} = 0$ , is the *quasiparticle* basis  $\{|\xi\rangle\}_{\xi=0,1,2,\dots}$  consisting of eigenstates of the projected Hamiltonian (Eqs. (6)–(8)).<sup>64</sup> Therefore, we consider the population relaxation dynamics in this preferred basis.

After introducing the quasiparticle energies  $\hbar\omega_{\bar{\xi}}$  and further adopting the interaction representation for the

density operator, i.e.  $\tilde{\rho}_{\bar{\xi}'\bar{\xi}}(t) = e^{-i\omega_{\bar{\xi}\bar{\xi}'}t} \rho_{\bar{\xi}\bar{\xi}'}(t)$  with  $\omega_{\bar{\xi}\bar{\xi}'} = \omega_{\bar{\xi}} - \omega_{\bar{\xi}'}$ , we recast Liouville Eq. (30) in the absence of optical pulse ( $\hat{V}(t) = 0$ ) to the quasiparticle basis. This results in the Redfield equation

$$\dot{\tilde{\rho}}_{\bar{\xi}\bar{\xi}}(t) = \sum_{\bar{\xi}'\bar{\xi}'} e^{-i(\omega_{\bar{\xi}\bar{\xi}'} - \omega_{\bar{\xi}'\bar{\xi}'})t} \mathcal{R}_{\bar{\xi}\bar{\xi};\bar{\xi}'\bar{\xi}'} \tilde{\rho}_{\bar{\xi}'\bar{\xi}'}(t), \quad (34)$$

where  $\mathcal{R}_{\bar{\xi}\bar{\xi};\bar{\xi}'\bar{\xi}'}$  is the relaxation tensor.

The interaction representation allows us to apply the so called secular approximation eliminating the fast oscillating terms containing  $\omega_{\bar{\xi}\bar{\xi}} - \omega_{\bar{\xi}'\bar{\xi}'} \neq 0$ . Respectively, the remaining Redfield tensor components<sup>65</sup>

$$R_{\bar{\xi}\bar{\xi};\bar{\xi}'\bar{\xi}'} = -\delta_{\bar{\xi}\bar{\xi}'} \sum_{\bar{\sigma} \neq \bar{\xi}} \Gamma_{\bar{\sigma}\bar{\xi}} + \Gamma_{\bar{\xi}\bar{\xi}'}, \quad (35)$$

$$R_{\bar{\xi}\bar{\xi};\bar{\xi}\bar{\xi}} = -\frac{1}{2} \sum_{\bar{\sigma} \neq \bar{\xi}} \Gamma_{\bar{\sigma}\bar{\xi}} - \frac{1}{2} \sum_{\bar{\sigma} \neq \bar{\xi}} \Gamma_{\bar{\sigma}\bar{\xi}} - \gamma_{\bar{\xi}\bar{\xi}}, \quad (36)$$

correspond to uncoupled equations for the population relaxation and coherence dephasing. Eqs. (35) and (36) contain the population relaxation and pure dephasing rates

$$\Gamma_{\bar{\xi}\bar{\xi}'} = \frac{1}{\hbar^2} \sum_{\alpha\alpha'} Y_{\bar{\xi}\bar{\xi}';\alpha} Y_{\bar{\xi}'\bar{\xi};\alpha'} C_{\alpha\alpha'}(\omega_{\bar{\xi}\bar{\xi}'}), \quad (37)$$

$$\begin{aligned} \gamma_{\bar{\xi}\bar{\xi}} = & \frac{1}{\hbar^2} \sum_{\alpha\alpha'} (Y_{\bar{\xi}\bar{\xi};\alpha} - Y_{\bar{\xi}\bar{\xi};\alpha'}) \\ & \times (Y_{\bar{\xi}\bar{\xi};\alpha'} - Y_{\bar{\xi}\bar{\xi};\alpha}) \tilde{C}'_{\alpha\alpha'}(0), \end{aligned} \quad (38)$$

respectively. Here,  $\tilde{C}_{\alpha\alpha'}(\omega)$  denotes the Fourier transform of the phonon correlation function  $C_{\alpha\alpha'}(\tau) = \langle e^{\hat{H}_p\tau} \hat{q}_\alpha e^{-i\hat{H}_p\tau} \hat{q}_{\alpha'} \rangle_{eq}$ , and contains real  $C'_{\alpha\alpha'}(\omega)$  and imaginary  $C''_{\alpha\alpha'}(\omega)$  parts. Explicit representation for the correlation function depends on the adopted form of  $H_p$ , i.e. on specific relaxation model.

The products of the off-diagonal quasiparticle-phonon coupling constants entering the population relaxation rate (Eq. (37)) can be expressed in terms of the exciton-phonon matrix elements entering Eq. (33) as

$$Y_{\bar{\xi}\bar{\xi}';\alpha} Y_{\bar{\xi}'\bar{\xi};\alpha'} = \sum_{ll'rr'} \bar{\Lambda}_{lr}(\omega_{\bar{\xi}}) \bar{\Lambda}_{l'r'}(\omega_{\bar{\xi}'}) Y_{ll';\alpha} Y_{r'r';\alpha'}. \quad (39)$$

Finally, a matrix element of the diagonal quasiparticle-phonon coupling determining the pure dephasing rate (Eq. (37)) is

$$Y_{\bar{\xi}\bar{\xi};\alpha} = \sum_{lr} \bar{\Lambda}_{lr}(\omega_{\bar{\xi}}) Y_{lr;\alpha}. \quad (40)$$

In Eqs. (39) and (40),  $\bar{\Lambda}_{lr}(\omega_{\bar{\xi}}) = \lim_{\gamma \rightarrow 0} \text{res}\{G_{lr}(\tilde{\omega}_{\bar{\xi}})\}$  is the transition amplitudes given by the Green function residues in the limit of infinitesimal imaginary part  $\gamma$  of the poles.<sup>70</sup> Here and below, we use an agreement that the summation indices for single- and bi-exciton states



(particularly those in Eqs. (39) and (40)) run over all single- and bi-exciton states, unless the superscripts  $x$  or  $xx$  constraining their range are used (e.g. in Eq. (33) for  $Y_{ab;\alpha}^x$ ,  $Y_{kl;\alpha}^{xx}$ , and  $Y_{ak;\alpha}^{x,xx}$ ).

The dependence of the population relaxation rate (Eqs. (37) and (39)) on the transition amplitude indicates that the exciton scattering processes are involved into the phonon-assisted cooling. Some of them as we demonstrated in Sec. II C change the multiplicity of the initial states, and, therefore, can be considered as generalized impact ionization and Auger recombination processes. Accordingly, we argue that the phonon-assisted cooling and impact ionization dynamics giving rise to CM are generally entangled. However, we demonstrate in Sec. IV, that the *intraband* phonon-assisted cooling and the interband by their nature impact ionization and Auger recombination processes can be partitioned in the limit of weak Coulomb coupling.

By applying the secular approximation, we significantly simplify the description of the phonon assisted dynamics. However, validity of the adopted approximation in NCs is based on the following delicate interplay between the number of quantum states and their energy separation: In the region of high DOS some closely lying levels may have  $\omega_{\xi\xi} - \omega_{\xi'\xi'} \approx 0$  potentially leading to the breakdown of the secular approximation. On the other hand, we expect that due to the same high DOS, there are enough terms in the sum of Eq. (34) containing these slow-oscillating phases to cancel out their contributions. Therefore, the adopted secular approximation should be validated during numerical simulations for specific materials.

## B. Photoexcited population dynamics and QE

Central quantity describing CM is QE which can be calculated as

$$QE = \frac{2N_{xx}(\tau) + N_x(\tau)}{N_{xx}(\tau) + N_x(\tau)}, \quad (41)$$

where  $N_x(\tau) = \text{tr} \hat{\rho}^x(\tau)$  and  $N_{xx}(\tau) = \text{tr} \hat{\rho}^{xx}(\tau)$  are total single-exciton and bi-exciton populations, respectively. Their dependence on the delay time  $\tau$  measured from the center of the pump pulse allows for comparison of QE of photogeneration event and total QE after the population relaxation. The latter is typically measured in optical experiment.

The calculation of QE requires solution of Liouville equation given by Eq. (30) for the single- and bi-exciton populations  $\rho_s$ . Solution of Eq. (30) can be obtained by noticing that the coupling between optical field and the exciton states is weak compared to the transition energies. This results in the second order perturbation expression associated with the double-sided Feynman diagram presented in Fig. 5 (a).<sup>56</sup> Resulting population

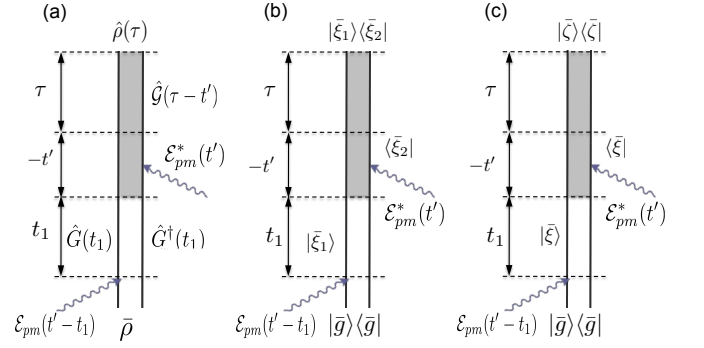


FIG. 5: Double-sided Feynman diagram representation of the nonequilibrium density operator  $\hat{\rho}(\tau)$  prepared by the pump pulse and propagated during delay time  $\tau$ . Times  $t_1$  and  $t'$ , are the integration variables, and  $\bar{\rho}$  is the equilibrium density operator.  $\hat{\rho}(\tau)$  can be partitioned into two components reflecting contributions of (b) the quasiparticle coherences and (c) the quasiparticle populations.

matrix element is

$$\begin{aligned} \rho_s(\tau) = & -2\hbar^{-2} \text{Re} \sum_{l_0 l_1 l_2} \sum_{r_0 r_1 r_2} \quad (42) \\ & \mu_{l_1 l_0} \bar{\rho}_{l_0 r_0} \mu_{r_1 r_2} \\ & \times \int_{-\infty}^{\infty} dt' \int_0^{\infty} dt_1 \mathcal{G}_{ss, l_2 r_2}(\tau - t') \\ & \times G_{l_2 l_1}(t_1) G_{r_1 r_0}^*(t_1) \\ & \times \mathcal{E}_{pm}(t') \mathcal{E}_{pm}^*(t - t_1) e^{i\omega_{pm} t_1}, \end{aligned}$$

where  $G_{lr}(t)$  is a matrix element of the projected propagator (Sec. II B), and  $\mathcal{G}_{ll, l_3 r_1}(\tau - t')$  is a matrix element of the Redfield equation (Eq. (34)) transformed to the bare single- and bi-exciton basis. Finally  $\bar{\rho}_{lr}$  is a matrix element of the equilibrium density operator<sup>71</sup>

$$\begin{aligned} \bar{\rho} = & |x_0\rangle\langle x_0| \quad (43) \\ & + \sum_{k \geq 1} \left( |x_0\rangle \bar{\Lambda}_{0,k}^{x,xx} \langle xx_k| - |xx_k\rangle \bar{\Lambda}_{k,0}^{xx,x} \langle x_0| \right) \\ & + \sum_{a \geq 1} \left( |x_0\rangle \bar{\Lambda}_{0a}^x \langle x_a| + |x_a\rangle \bar{\Lambda}_{a0}^x \langle x_0| \right). \end{aligned}$$

with

$$\begin{aligned} \bar{\Lambda}_{0,k}^{x,xx} = & -\bar{\Lambda}_{k,0}^{xx,x} = -\frac{V_{0,k}^{x,xx}}{\hbar\omega_k}, \quad (44) \\ \bar{\Lambda}_{0a}^x = & \bar{\Lambda}_{a0}^x = \sum_{k \geq 1} \frac{V_{0,k}^{x,xx} V_{k,a}^{xx,x}}{\hbar^2 \omega_a \omega_k^{xx}}. \end{aligned}$$

Equation (42) can be used for numerical calculations of QE. This expression is quite general meaning that its form does not assume that the secular approximation allowing to separate the coherence and population relaxation dynamics is used. For further analysis, we partition the contributions to  $\rho_s(\tau)$  induced by the optical excitation of the quasiparticle populations and coherences. For



this purpose, we represent the time-dependent matrix elements of the projected propagator as

$$G_{lr}(t) = \sum_{\bar{\xi}} \Lambda_{lr}(\omega_{\bar{\xi}}) e^{-i\tilde{\omega}_{\bar{\xi}} t}, \quad (45)$$

where the quasiparticle complex frequencies  $\tilde{\omega}_{\bar{\xi}} = \omega_{\bar{\xi}} - i\gamma_{\bar{\xi}}$  are the poles of  $G_{lr}(\omega)$ , and  $\Lambda_{lr}(\omega_{\bar{\xi}}) = \text{res}\{G_{lr}(\tilde{\omega}_{\bar{\xi}})\}$  is complex transition amplitude given by the Green function residue.<sup>72</sup> Eq. (45) clarifies the physical meaning of the latter quantity showing that this is a probability amplitude for the transition between  $l$  and  $r$  states in the single- and bi-exciton basis associated with the propagation of quasiparticle state  $|\bar{\xi}\rangle$ .

Substitution of Eq. (45) into Eq. (42) and partitioning the quasiparticle coherence and population dynamics (secular approximation) allows us to recast  $\rho_s$  into the sum of two terms

$$\rho_s(\tau) = c_s(\tau) + n_s(\tau). \quad (46)$$

Here, the first term corresponding to the double-sided diagram shown in Fig. 5 (b), describes the contribution of the quasiparticle coherences

$$c_s(\tau) = \sum_{\bar{\xi}_1 \bar{\xi}_2} \sum_{s_0} \mu_{ss_0}(\bar{\xi}_1) \mu_{ss_0}^*(\bar{\xi}_2) e^{-i\tilde{\omega}_{\bar{\xi}_1 \bar{\xi}_2} \tau} \quad (47)$$

$$\times \mathcal{I}(\tilde{\omega}_{\bar{\xi}_1 0} - \omega_{pm}; \tilde{\omega}_{\bar{\xi}_2 0} - \omega_{pm}),$$

where  $\mu_{ss_0}(\bar{\xi}_1)$  denotes projection of the transition dipole moment between the quasiparticle ground and  $\bar{\xi}$ -th states onto single-/bi-exciton states

$$\mu_{ss_0}(\bar{\xi}) = \sum_{l_1 l_2} \Lambda_{sl_1}(\omega_{\bar{\xi}}) \mu_{l_1 l_2} \bar{\rho}_{l_2 s_0}, \quad (48)$$

with the matrix elements  $\bar{\rho}_{l_2 s_0}$  of the equilibrium density operator (Eqs. (44)).<sup>73</sup> Note that  $\mu_{ss_0}(\bar{\xi})$  mixes interband and intraband dipole transitions entering the optical interaction term of the Hamiltonian (Eq. (28)).

Pulse self-convolution function in Eq. (47) is

$$\mathcal{I}(\tilde{\omega}_{\bar{\xi}_1 0} - \omega_{pm}; \tilde{\omega}_{\bar{\xi}_2 0} - \omega_{pm}) = \frac{1}{\hbar^2} \int_{-\infty}^{\infty} dt' \int_0^{\infty} dt_1$$

$$\times \theta(\tau - t') e^{i\tilde{\omega}_{\bar{\xi}_1 \bar{\xi}_2} t'} \left[ e^{-i(\tilde{\omega}_{\bar{\xi}_1 0} - \omega_{pm}) t_1} \right. \quad (49)$$

$$\left. + e^{i(\tilde{\omega}_{\bar{\xi}_2 0} - \omega_{pm}) t_1} \right] \mathcal{E}_{pm}(t') \mathcal{E}_{pm}(t' - t_1),$$

and depends on the coherence between the quasiparticle excited and ground states  $\tilde{\omega}_{\bar{\xi}_i, 0} = \tilde{\omega}_{\bar{\xi}_i} - \tilde{\omega}_0 - \gamma_{\bar{\xi}_i 0}$ , and on the excited state coherences characterized by  $\tilde{\omega}_{\bar{\xi}_i, \bar{\xi}_j} = \tilde{\omega}_{\bar{\xi}_i} - \tilde{\omega}_{\bar{\xi}_j} - \gamma_{\bar{\xi}_i \bar{\xi}_j}$  where the dephasing rates  $\gamma_{\bar{\xi}_i g}$  and  $\gamma_{\bar{\xi}_i \bar{\xi}_j}$  are determined by Eq. (38).

The second term in Eq. (46), represented by the double-sided diagram in Fig. 5 (c), describes the contribution of the quasiparticle populations

$$n_s(\tau) = \sum_{lr} \sum_{\bar{\xi} \bar{\zeta}} [\bar{\Lambda}_{ss}(\omega_{\bar{\zeta}}) \bar{\mathcal{G}}_{\bar{\zeta}, \bar{\xi}}(\tau) \bar{\Lambda}_{lr}(\omega_{\bar{\xi}})] \quad (50)$$

$$\mu_{ls_0}(\bar{\xi}) \mu_{rs_0}^*(\bar{\xi}) \mathcal{I}(\tilde{\omega}_{\bar{\xi} 0} - \omega_{pr}).$$

Here,  $\bar{\Lambda}_{lr}(\omega_{\bar{\xi}}) = \lim_{\gamma \rightarrow 0} \Lambda_{lr}(\omega_{\bar{\xi}})$ , and  $\bar{\mathcal{G}}_{\bar{\zeta}, \bar{\xi}}(\tau) \equiv \mathcal{G}_{\bar{\zeta} \bar{\zeta}, \bar{\xi} \bar{\xi}}(\tau)$  denotes the quasiparticle population relaxation component of the Green function associated with the Redfield equation. This Green function can be found in a standard way by using the eigenstates and eigenvalues of the Redfielded operator (Eq. (35)).<sup>56,64,66</sup> If high DOS does not allow to diagonalize the relaxation operator then  $n_s(0)$  should be considered as the initial condition for numerical solution of the Redfield equation (Eq. (34)).<sup>74</sup> Finally, pulse self-convolution function in Eq. (50) simplifies to the form

$$\mathcal{I}(\tilde{\omega}_{\bar{\xi} 0} - \omega_{pm}) = \frac{2}{\hbar^2} \int_{-\infty}^{\infty} dt' \int_0^{\infty} dt_1 e^{-\gamma_{\bar{\xi} g} t_1} \quad (51)$$

$$\times \cos[(\omega_{\bar{\xi} 0} - \omega_{pm}) t_1] \mathcal{E}_{pm}(t') \mathcal{E}_{pm}(t' - t_1),$$

where we neglect the population relaxation processes during the interaction with the pulse.

The representation given by Eqs. (46)–(51), provides connection with the sum-over-eigenstates representation shown in Fig. 5 (b) and (c). In this representation there is an additional Liouville space pathway contribution to the single- and bi-exciton populations associated with the propagation of the ground state wave packet.<sup>56</sup> This term can, in principle, contribute to the CM dynamics if Coulomb coupling between the vacuum and bi-exciton states is strong enough to make the lowest excited state energy to be comparable with thermal energy  $k_B T$ , i.e.  $V^{xx,0} \sim 2E_g - k_B T$ . Since, the latter condition is not satisfied in NCs where typically  $E_g \gg V^{xx,0} \gg k_B T$ , we do not consider this pathway.

Finally, one can expect that the contribution to QE associated with the excitation of the quasiparticle coherences (Eq. (47)) can become negligible compared to the quasiparticle populations (Eq. (50)). This could happen, since spectral widths of ultrafast pump pulse allows to excite significantly large number of states (Fig. 4(a)) whose phases entering Eq. (47) through Eq. (49) add destructively. This assumption can be checked for specific materials through numerical evaluation of the related terms.

#### IV. LIMIT OF WEAK COULOMB COUPLING

In this section, we consider Exciton Scattering Model, developed in Secs. II and III, in the limiting case of weak Coulomb coupling. This limit is important for applications and assumes that the Coulomb matrix elements between single- and bi-exciton states are much smaller than the energy difference between these levels and/or the levels broadening, i.e.  $V_{a,k}^{xx,xx} \ll \hbar (|\omega_a^x - \omega_k^{xx}|, \gamma_{a,k}^{xx,xx})$ . As we demonstrate below, both carrier photogeneration and population relaxation dynamics can be described as no higher than second order processes in the Coulomb expansion. For this purpose, we use Eqs. (46)–(51), with the Green function components calculated in the adopted limit.

### A. Time-domain Green function

To find the Green functions, we, first, represent the single-exciton ( $\bar{n} = x$ ) and bi-exciton ( $\bar{n} = xx$ ) free propagator (Eq. (16)) as

$$g_{kl}^{\bar{n}}(\omega) = \frac{i\delta_{kl}}{(\omega - \tilde{\omega}_k^{\bar{n}})}, \quad (52)$$

where a complex frequency  $\tilde{\omega}_k^{\bar{n}} = \omega_k^{\bar{n}} - i\gamma_k^{\bar{n}}$  contains  $k$ -th frequency  $\omega_k^{\bar{n}}$  from the projected Hamiltonian (Eq. (7)), and related dephasing rate  $\gamma_k^{\bar{n}}$ .

If the interband Coulomb interaction is weak, the CM dynamics becomes dominated by the Born interband scattering represented by the first vertex diagram in Fig. 3 (c). According to Eq. (26), the scattering matrix elements in Born approximation become

$$T_{a,k}^{x,xx}(\omega) = (i\hbar)^{-1} V_{a,k}^{x,xx}. \quad (53)$$

Furthermore, the leading contribution to the even-order scattering matrix (Fig. 3 (a) and (b)) comes from the self-energy, and according to Eqs. (24) and (25), its single- and bi-exciton components become

$$T_{ab}^x(\omega) = i \sum_{k \geq 1} \frac{V_{a,k}^{x,xx} V_{k,b}^{xx,x}}{\hbar^2(\omega - \tilde{\omega}_k^{xx})}, \quad (54)$$

$$T_{kl}^{xx}(\omega) = i \sum_{a \geq 0} \frac{V_{k,a}^{xx,x} V_{a,l}^{xx,x}}{\hbar^2(\omega - \tilde{\omega}_a^x)}, \quad (55)$$

respectively.

To calculate the time-dependent Green function, we substitute Eqs. (52)–(55) into Eqs. (21)–(23). Further use of Fourier transformation (Eq. (18)) leads to the following expressions

$$G_{ab}^x(t) = \delta_{ab} e^{-i\tilde{\omega}_a^x t} + \Lambda_{ab}^x \left( e^{-i\tilde{\omega}_a^{xx} t} - e^{-i\tilde{\omega}_b^x t} \right) \quad (56)$$

$$- \sum_{k \geq 1} \Lambda_{a,k}^{x,xx} \Lambda_{k,b}^{xx,x} e^{-i\tilde{\omega}_k^{xx} t},$$

$$G_{kl}^{xx}(t) = \delta_{kl} e^{-i\tilde{\omega}_k^{xx} t} + \Lambda_{kl}^{xx} \left( e^{-i\tilde{\omega}_k^{xx} t} - e^{-i\tilde{\omega}_l^x t} \right) \quad (57)$$

$$- \sum_{a \geq 0} \Lambda_{k,a}^{xx,x} \Lambda_{a,l}^{xx,x} e^{-i\tilde{\omega}_a^x t},$$

$$G_{a,k}^{x,xx}(t) = \Lambda_{a,k}^{x,xx} \left( e^{-i\tilde{\omega}_a^x t} - e^{-i\tilde{\omega}_k^{xx} t} \right). \quad (58)$$

Here, the shorthand notations for the renormalized complex single- and bi-exciton *quasiparticle* frequencies

$$\tilde{\omega}_a^x = \tilde{\omega}_a^x + \sigma_a^x \quad (59)$$

$$\tilde{\omega}_k^{xx} = \tilde{\omega}_k^{xx} + \sigma_k^{xx}, \quad (60)$$

are used, respectively. They contain the following self-energy corrections

$$\sigma_a^x = \sum_{k \geq 1} \frac{V_{a,k}^{x,xx} V_{k,a}^{xx,x}}{\hbar^2(\tilde{\omega}_a^x - \tilde{\omega}_k^{xx})} \quad (61)$$

$$\sigma_k^{xx} = \sum_{a \geq 0} \frac{V_{k,a}^{xx,x} V_{a,k}^{xx,x}}{\hbar^2(\tilde{\omega}_k^{xx} - \tilde{\omega}_a^x)}. \quad (62)$$

Finally, the transition amplitudes in Eqs. (56)–(58) are

$$\Lambda_{ab}^x = (1 - \delta_{ab}) \sum_{k \geq 1} \frac{V_{a,k}^{x,xx} V_{k,b}^{xx,x}}{\hbar^2(\tilde{\omega}_a^x - \tilde{\omega}_k^{xx})(\tilde{\omega}_a^x - \tilde{\omega}_b^x)} \quad (63)$$

$$\Lambda_{kl}^{xx} = (1 - \delta_{kl}) \sum_{a \geq 0} \frac{V_{k,a}^{xx,x} V_{a,l}^{xx,x}}{\hbar^2(\tilde{\omega}_k^{xx} - \tilde{\omega}_a^x)(\tilde{\omega}_k^{xx} - \tilde{\omega}_l^x)} \quad (64)$$

$$\Lambda_{a,k}^{x,xx} = \frac{V_{a,k}^{x,xx}}{\hbar(\tilde{\omega}_a^x - \tilde{\omega}_k^{xx})}. \quad (65)$$

Obtained representation for the time-domain Green function (Eqs. (56)–(65)) is accurate up to the second order terms in the interband Coulomb interaction. Next, these expressions are employed to provide the leading contributions to the single- and bi-exciton photogenerated populations and to derive a set of rate equations for the population relaxation.

### B. Single- and bi-exciton photogeneration

Use of the Green functions represented by Eqs. (56)–(65) together with Eqs. (46)–(51) results in the following form of the photo-generated single-exciton population

$$\rho_a^x = n_a^{x(0)} + n_a^{x(1)} + n_a^{x(2)} + c_a^{x(2)}, \quad (66)$$

where zeroth-, first-, and second-order terms describing the contributions due to optically prepared quasiparticle populations are

$$n_a^{x(0)} = |\mu_{a0}^x|^2 \mathcal{I}(\tilde{\omega}_a^x - \omega_{pm}), \quad (67)$$

$$n_a^{x(1)} = 2Re \sum_{k \geq 1} \mu_{a,k}^{x,xx} \Lambda_{k,0}^{xx,x} \mu_{0a}^x \mathcal{I}(\tilde{\omega}_a^x - \omega_{pm}), \quad (68)$$

$$n_a^{x(2)} = \left\{ \left| \sum_{k \geq 1} \mu_{a,k}^{x,xx} \bar{\Lambda}_{k,0}^{xx,x} \right|^2 + \sum_{k \geq 1} \left| \mu_{a0}^x \bar{\Lambda}_{0,k}^{xx,x} \right|^2 \right. \quad (69)$$

$$+ 2Re \sum_{b \geq 0} (\mu_{0a}^x \Lambda_{ab}^x \mu_{b0}^x + \mu_{0a}^x \mu_{ab}^x \bar{\Lambda}_{b0}^x)$$

$$\left. + 2Re \sum_{kl \geq 1} \mu_{0a}^x \Lambda_{a,k}^{x,xx} \mu_{kl}^{xx,x} \bar{\Lambda}_{l,0}^{xx,x} \right\} \mathcal{I}(\tilde{\omega}_a^x - \omega_{pm}),$$

respectively. They contain the pulse self-convolution function (Eq. (51)) which is resonant only at *single*-exciton quasiparticle frequencies.

In contrast, the quasiparticle coherences contributing to  $\rho_a^x$  contain both single- and bi-exciton reosnanses

$$c_a^{x(2)} = -2Re \sum_{b \geq 1} \mu_{0a}^x \Lambda_{ab}^x \mu_{b0}^x \quad (70)$$

$$\times \mathcal{I}(\tilde{\omega}_b^x - \omega_{pm}; \tilde{\omega}_a^x - \omega_{pm})$$

$$- 2Re \sum_{k \geq 1} \mu_{0a}^x \Lambda_{a,k}^{x,xx}$$

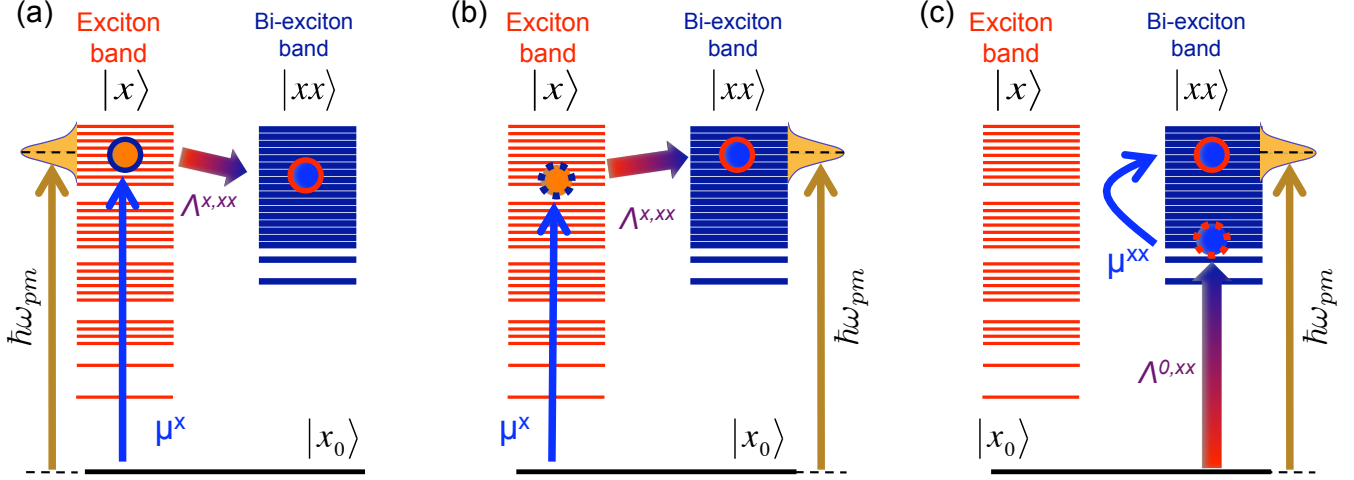


FIG. 6: Bi-exciton photogeneration pathways in the weak Coulomb limit. Panels (a) and (b) show two components of the pathway involving the vacuum to single-exciton dipole transition ( $\mu^x$ ) and the interband Born scattering ( $\Lambda^{x,xx}$ ). In panel (a), the intraband transition is in the resonance with the optical pulse ( $\hbar\omega_{pm}$ ) but final bi-exciton state energy is distributed around  $\hbar\omega_{pm}$  according to the non-zero components of  $\Lambda^{x,xx}$ . Situation in panel (b) is the opposite, where the single-exciton is virtual and final bi-exciton state is in the resonance with the optical pulse. (c) The pathway containing production of virtual bi-exciton state due to the Born scattering from the exciton vacuum ( $\Lambda^{0,xx}$ ) followed by the intraband dipole transition  $\mu^{xx}$ . Here, final bi-exciton state is in the resonance with the optical pulse.

$$\begin{aligned} & \times \left( \sum_{l \geq 1} \mu_{kl}^{xx} \bar{\Lambda}_{l,0}^{xx,x} + \sum_{b \geq 1} \Lambda_{k,b}^{xx,x} \mu_{b0}^x \right) \\ & \times \mathcal{I}(\bar{\omega}_k^{xx} - \omega_{pm}; \bar{\omega}_a^x - \omega_{pm}), \end{aligned} \quad \times \left[ \sum_{b \geq 1} \Lambda_{k,b}^{xx,x*} \mu_{b0}^{x*} + \sum_{l \geq 1} \mu_{kl}^{xx*} \bar{\Lambda}_{l,0}^{xx,x} \right] \\ & \times \mathcal{I}(\bar{\omega}_a^x - \omega_{pm}; \bar{\omega}_k^{xx} - \omega_{pm}).$$

entering pulse self-convolution function (Eq. (49)). Although Eqs. (67)–(70) are important for numerical calculations of QE, we do not discuss scattering pathways associated with each term, since these pathways carry no information on the CM dynamics.

The photogenerated bi-exciton population in the weak Coulomb limit according to Eqs. (46)–(51) and Eqs. (56)–(65) is

$$\rho_k^{xx} = n_k^{xx(2)} + c_k^{xx(2)}, \quad (71)$$

where the quasiparticle population contribution is

$$\begin{aligned} n_k^{xx(2)} &= \sum_{a \geq 1} \left| \Lambda_{k,a}^{xx,x} \mu_{a0}^x \right|^2 \mathcal{I}(\bar{\omega}_a^x - \omega_{pm}) \\ &+ \left| \sum_{a \geq 1} \Lambda_{k,a}^{xx,x} \mu_{a0}^x + \sum_{l \geq 1} \mu_{kl}^{xx} \bar{\Lambda}_{l,0}^{xx,x} \right|^2 \\ &\times \mathcal{I}(\bar{\omega}_k^{xx} - \omega_{pm}), \end{aligned} \quad (72)$$

and the quasiparticle coherence contribution is

$$\begin{aligned} c_k^{xx(2)} &= -2\text{Re} \sum_{(a \neq b) \geq 1} \mu_{0a}^x \Lambda_{a,k}^{x,xx} \Lambda_{k,b}^{xx,x*} \mu_{b0}^{x*} \\ &\times \mathcal{I}(\bar{\omega}_a^x - \omega_{pm}; \bar{\omega}_b^x - \omega_{pm}) \\ &- 2\text{Re} \sum_{a \geq 1} \mu_{0a}^x \Lambda_{a,k}^{x,xx} \end{aligned} \quad (73)$$

Note that Eqs. (71)–(73) contain only second-order Coulomb terms.

Equation (72) has a clear physical interpretation illustrated in Fig. 6 where two interfering photogeneration pathways can be distinguished: The first pathway is shown in panels (a) and (b) and involves the vacuum to single-exciton dipole transition ( $\mu_{0a}^x$ ) and interband Born scattering ( $\Lambda_{a,k}^{x,xx}$ ). The product  $\mu_{0a}^x \Lambda_{a,k}^{x,xx}$  of the latter quantities enter the first and second summations over single-exciton index  $a$ . These sums describe the redistribution of the bare single-exciton oscillator strength between the quasiparticle single-exciton (panel (a)) and bi-exciton (panel (b)) resonances. The second pathway, shown in panel (c), is represented by the last sum over bi-exciton index  $l$ . Here, the optical transition to a quasiparticle bi-exciton resonance is a combination of Born scattering event between the vacuum and a bi-exciton state ( $\bar{\Lambda}_{0,k}^{x,xx}$ ) and the bi-exciton intraband transition ( $\mu_{kl}^{xx}$ ). Comparison of Eqs. (72) and (73) shows that the latter contains the interference of similar scattering pathways.

### C. Population relaxation

To derive a set of rate equations for the population relaxation, we first represented the Redfield equation (Eq. (34)) in the bare single- and bi-exciton basis. In

this representation populations and coherences are coupled. We eliminated the coherences and obtained a memory kernel depending on the interband Coulomb coupling. We further applied the Markov approximation to the kernel based on the main assumption that the Coulomb interaction is much smaller than the line width rising from the pure dephasing processes. This procedure resulted in the following set of rate equations

$$\dot{\rho}_a^x = - \sum_m k_{a,m}^{x,xx} (\rho_a^x - \rho_m^{xx}) \quad (74)$$

$$- \sum_b (\Gamma_{ba}^x \rho_a^x - \Gamma_{ab}^x \rho_b^x),$$

$$\dot{\rho}_k^{xx} = - \sum_b k_{b,k}^{x,xx} (\rho_k^{xx} - \rho_b^x) \quad (75)$$

$$- \sum_m (\Gamma_{mk}^{xx} \rho_k^{xx} - \Gamma_{km}^{xx} \rho_m^{xx}).$$

Here, the interband scattering and the intraband phonon-induced population cooling are described by different terms indicating that in the weak Coulomb limit these two processes are uncoupled (Fig. 7). Specifically, the first term in the r.h.s. of each equation describes the interband population transfer due to the impact ionization and Auger recombination processes. Associated population transfer rate, rising from the Markov kernel appeared during the coherence elimination, is

$$k_{a,n}^{x,xx} = \frac{2}{\hbar^2} |V_{a,k}^{x,xx}|^2 \frac{\gamma_{a,k}^{x,xx}}{(\omega_a^x - \omega_k^{xx})^2 + (\gamma_{a,k}^{x,xx})^2}, \quad (76)$$

where  $\gamma_{a,n}^{x,xx}$  is a pure dephasing rate.

The second term in the r.h.s. of each Eq. (74) and (75), describes phonon-assisted cooling. Entering there, population decay rates can be obtained from general expression given by Eq. (37) and (39), where we set  $\bar{\Lambda}_{ab}(\omega_x) = \delta_{ab}$ ,  $\bar{\Lambda}_{kl}(\omega_{xx}) = \delta_{kl}$ , and  $\bar{\Lambda}_{ak}(\omega_{x,xx}) = 0$ . These transition amplitudes rise from *zero*-order Coulomb terms of the Green functions given by Eqs. (56)–(58). The remaining second order transition amplitudes are dropped, since together with the exciton-phonon couplings their net contribution to the rates becomes negligibly small.

Since, during the transformation from the quasiparticle representation back to bare single- and bi-exciton representation one has to keep only zeroth-order Coulomb terms, the form of the population relaxation rates does not change. As a result, their expressions are

$$\Gamma_{ab}^x = \frac{1}{\hbar^2} \sum_{\alpha\alpha'} Y_{ab;\alpha}^x Y_{ab;\alpha'}^x C_{\alpha\alpha'} (\omega_a^x - \omega_b^x), \quad (77)$$

$$\Gamma_{kl}^{xx} = \frac{1}{\hbar^2} \sum_{\alpha\alpha'} Y_{kl;\alpha}^{xx} Y_{kl;\alpha'}^{xx} C_{\alpha\alpha'} (\omega_k^{xx} - \omega_l^{xx}), \quad (78)$$

where the phonon correlation function  $\tilde{C}_{\alpha\alpha'}(\omega)$  is defined in Sec. III A, and the exciton-phonon coupling constants  $Y_{ab;\alpha}^x$  and  $Y_{kl;\alpha}^{xx}$  are defined by Eqs. (B3) and (B4), respectively.<sup>75</sup> Similarly, the following expression for the

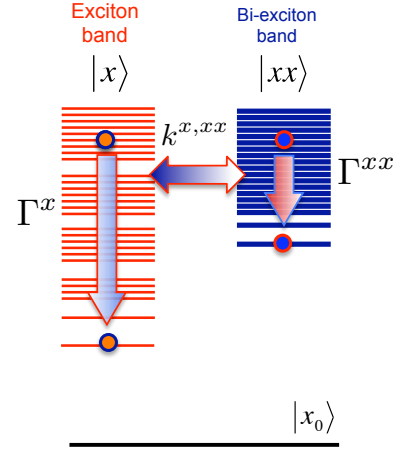


FIG. 7: Population relaxation in the weak Coulomb limit consists of uncoupled interband Auger recombination and impact ionization processes with rate  $k^{x,xx}$ , and the intraband phonon-induced cooling with rates  $\Gamma^x$  and  $\Gamma^{xx}$ .

pure dephasing rate immediately follows from Eqs. (38), (40), (56), and (57)

$$\gamma_{a,n}^{x,xx} = \frac{1}{\hbar^2} \sum_{\alpha\alpha'} (Y_{aa;\alpha}^x - Y_{nn;\alpha}^{xx}) \quad (79)$$

$$\times \left( Y_{aa;\alpha'}^x - Y_{nn;\alpha'}^{xx} \right) \tilde{C}'_{\alpha\alpha'}(0).$$

Finally, we outline the computational scheme for the evaluation of QE within the weak Coulomb limit. First, Eqs. (66)–(73) should be evaluated to find the initial conditions  $\rho_a^x(0)$  and  $\rho_k^{xx}(0)$  for the population relaxation. These density matrix elements can also be used to obtain QE (Eq. (41)) associated with the photogeneration processes. Next, starting with the latter boundary conditions, the wavepackets  $\rho_a^x(t)$  and  $\rho_k^{xx}(t)$  should be numerically propagated to the bottom of the single- and bi-exciton bands according to Eqs. (74) and (75) with the parameters defined by Eqs. (76)–(79). This provides input for the determination of the total QE.

## V. DISCUSSION AND CONCLUSIONS

In this section, we discuss connection of proposed Exciton Scattering Model with previously developed Coherent Superposition Model,<sup>46</sup> Direct Photogeneration Model,<sup>27,47</sup> and Impact Ionization Model<sup>49,50</sup>. We also comment on a general scheme for QE calculations in NCs and in bulk materials.

### A. Coherent Superposition Model

Coherent Superposition Model is a limit of Exciton Scattering Model, where just two states  $|x_c\rangle$  and  $|xx_c\rangle$  are coupled by the Coulomb matrix element  $V^{x,xx}$ , and

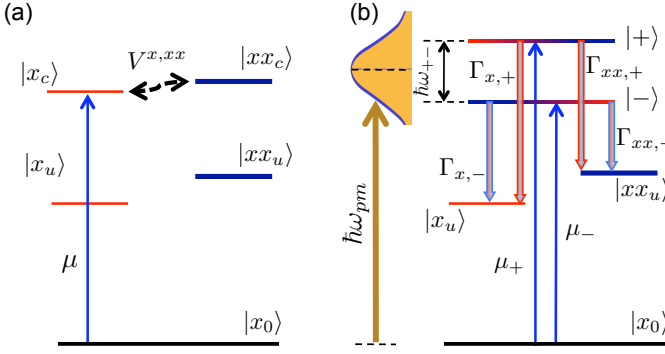


FIG. 8: Level diagram for Coherent Superposition model: (a) Bare single- and bi-exciton state representation where two states  $|x_c\rangle$  and  $|xx_c\rangle$  are coupled by Coulomb matrix element  $V^{x,xx}$ , and two states  $|x_u\rangle$  and  $|xx_u\rangle$  are uncoupled. Transition dipole  $\mu$  couples vacuum state with the upper single-exciton states. (b) Quasiparticle representation. Scattering processes correspond to the optical transitions with  $\mu_+ = \sqrt{\Lambda_+^x}\mu$  and  $\mu_- = \sqrt{\Lambda_-^x}\mu$ . In a short pulse limit, the pump spectral widths exceeds  $\hbar\omega_{+-}$ , and both the coherence and populations of  $|\pm\rangle$  states are prepared. Their projections back to the bare single- and bi-exciton populations are given by Eqs. (83) and (84). The population relaxation pathways with their rates entering Eqs. (83)–(86) are shown by the arrows pointed down.

two states  $|x_u\rangle$  and  $|xx_u\rangle$  are uncoupled as shown in Fig. 8 (a). There is also no coupling to the vacuum state. The coupled states are assumed to be almost degenerate, i.e.  $\hbar\omega_c^{xx} \sim \hbar\omega_c^x$ , leading to strong interaction condition  $\hbar|\omega_c^{xx} - \omega_c^x| \ll V^{x,x}$ . Details on the calculations of the scattering matrix components, single- and bi-exciton Green functions in the framework of Coherent Superposition Model are given in Appendix D. According to these calculations, strong Coulomb interaction corresponds to the splitting between coupled states, and formation of the quasiparticle states  $|\pm\rangle$  with energies  $\hbar\omega_{\pm}$  (Eq. (D5)) as illustrated in Fig. 8 (b). Another assumption used in the calculations is that the splitting  $\omega_{+-} = \omega_+ - \omega_-$  significantly exceeds the quasiparticle level broadening. These assumptions in our new notations reproduce the model proposed in Ref. 46

The authors of Ref. 46 adopted the phonon-assisted relaxation model containing uncoupled intraband relaxation pathways for single- and bi-excitons resulting in independent cooling within each manifold. We argue that these relaxation pathways are *coupled* since the Coulomb interaction is strong.<sup>62</sup> Furthermore, we pointed out in Sec. III A, that the relaxation equations should reproduce the equilibrium distribution function not for the bare single- and bi-exciton states but for the quasiparticle states. Another assumption used in Ref. 46 is that the dephasing rate between coupled states is fully determined by the population relaxation processes. However, the *pure dephasing* time in NCs is estimated to be several orders of magnitude shorter than the population relaxation time.<sup>67,68</sup> In this case, the dephasing rate is totally

due to the pure dephasing indicating separation of the timescales for the coherence and population dynamics.

The population relaxation rates from the quasiparticle states to the uncoupled single- and bi-exciton states, shown in Fig. 8 (b), immediately follow from Eqs. (37) and (39) with the transition amplitudes  $\Lambda_{\pm}^x$  and  $\Lambda_{\pm}^{xx}$  (Eqs. (D9) and (D10)) inserted. The rates are

$$\Gamma_{x,\pm} = \frac{1}{\hbar^2} \sum_{\alpha} [Y_{uc;\alpha}^x]^2 \Lambda_{\pm}^x C_{\alpha}(\omega_u^x - \omega_{\pm}), \quad (80)$$

$$\Gamma_{xx,\pm} = \frac{1}{\hbar^2} \sum_{\alpha} [Y_{uc;\alpha}^{xx}]^2 \Lambda_{\pm}^{xx} C_{\alpha}(\omega_u^{xx} - \omega_{\pm}), \quad (81)$$

where  $Y_{uc;\alpha}^x$  and  $Y_{uc;\alpha}^{xx}$  are the exciton-phonon interactions connecting the uncoupled and coupled states. Note that these expressions reproduce the uncoupled single- and bi-exciton relaxation rates only if Coulomb interaction is weak,  $\hbar|\omega_c^{xx} - \omega_c^x| \gg V^{x,x}$ .<sup>76</sup> The population transfer also exists *between* the quasiparticle states. However, for the sake of simplicity, we drop this pathway. The derivation of the pure dephasing rate  $\gamma_{+-}$  between the quasiparticle states is discussed in Appendix D.

Coherent Superposition Model consists of only one optical transition induced by the dipole moment  $\mu$  between the vacuum and coupled single-exciton state shown in panel (a) of Fig. 8. The scattering processes redistribute the oscillator strength so that both quasiparticle states become optically allowed as shown in panel (b). To observe the oscillations of the pump-probe signal (bleach) predicted by Coherent Superposition Model, the pulse duration should be less than the dephasing time and spectral widths of the pulse should exceed the level splitting  $\hbar\omega_{+-}$ . This condition is satisfied in the so called impulsive limit where the pulse self-convolution function becomes frequency independent<sup>77</sup>

$$\begin{aligned} \mathcal{I}_{sp} &\equiv \mathcal{I}_{sp}(\tilde{\omega}_{\pm} - \omega_{pm}) = \\ \mathcal{I}_{sp}(\tilde{\omega}_{+} - \omega_{pm}; \tilde{\omega}_{-} - \omega_{pm}) &= 4\hbar^{-2} \bar{\tau}_{pm}^2 [\mathcal{E}_{pm}^{(0)}]^2. \end{aligned} \quad (82)$$

Here,  $\mathcal{E}_{pm}^{(0)}$  is the amplitude of the pump pulse, and  $\bar{\tau}_{pm} = \sqrt{\pi}\tau_{pm}$  is effective pulse duration.

To find time-dependent populations of coupled states prepared by the short pulse, we use the expressions for corresponding density matrix components (Eqs. (D14), (D21), (D15), and (D21)) obtained in Appendix D along with Eq. (82). This results in the following populations of coupled single- and bi-exciton states

$$\rho_c^x(\tau) = A^2 \sum_{\xi=\pm} [\Lambda_{\xi}^x]^2 e^{-(\Gamma_{x,\xi} + \Gamma_{xx,\xi})\tau} \quad (83)$$

$$\begin{aligned} &+ 2A^2 \Lambda_+^x \Lambda_-^x \cos(\omega_{+-}\tau) e^{-\gamma_{+-}\tau}, \\ \rho_c^{xx}(\tau) &= A^2 \sum_{\xi=\pm} [\Lambda_{\xi}^{xx}]^2 e^{-(\Gamma_{x,\xi} + \Gamma_{xx,\xi})\tau} \quad (84) \\ &- 2A^2 \Lambda_+^x \Lambda_-^x \cos(\omega_{+-}\tau) e^{-\gamma_{+-}\tau}, \end{aligned}$$

respectively. The populations of the uncoupled states as the function of delay time  $\tau$  can be obtained from

Eqs. (D16) and (D17) together with Eq. (82)

$$\rho_u^x(\tau) = A^2 \sum_{\bar{\xi}=\pm} \frac{\Gamma_{x,\bar{\xi}} \Lambda_{\bar{\xi}}^x}{\Gamma_{x,\bar{\xi}} + \Gamma_{xx,\bar{\xi}}} \times \left\{ 1 - e^{-(\Gamma_{x,\bar{\xi}} + \Gamma_{xx,\bar{\xi}})\tau} \right\}, \quad (85)$$

$$\rho_u^{xx}(\tau) = A^2 \sum_{\bar{\xi}=\pm} \frac{\Gamma_{x,\bar{\xi}} \Lambda_{\bar{\xi}}^{xx}}{\Gamma_{x,\bar{\xi}} + \Gamma_{xx,\bar{\xi}}} \times \left\{ 1 - e^{-(\Gamma_{x,\bar{\xi}} + \Gamma_{xx,\bar{\xi}})\tau} \right\}. \quad (86)$$

Here,  $A = 2\mu\mathcal{E}^{(0)}\bar{\tau}_{pm}/\hbar$  is a dimensionless parameter;  $\Lambda_{\bar{\xi}}^x$ ,  $\Lambda_{\bar{\xi}}^{xx}$ , and  $\Lambda_{\bar{\xi}}^{xx}$  are transition amplitudes defined in Eqs. (D9)–(D11).

The oscillations predicted by Coherent Superposition Model exist only between coupled states, and have frequency equal to the quasiparticle level splitting  $\omega_{+-}$ . Specifically, they are described by the second term in Eqs. (83) and (84). Since, there is no oscillating term in the populations of the uncoupled states, oscillations of the bleach can be observed in experiment where the probe directly monitors time evolution of  $\rho_c^x$  and/or  $\rho_c^{xx}$ . In fact, the expression for bleach, given by Eq. (7) in Ref. 46, contains non-vanishing contribution of the coupled bi-exciton population.

Finally, we compare QE of the photogeneration event, and total QE after the population cooling. The photogeneration QE can be determined from Eqs. (41), (83), and (84) on the timescale longer than the dephasing occurs but shorter than the populations relax. This quantity reads

$$QE_{<} = \frac{12(V^{x,xx})^2 + (\omega_c^{xx} - \omega_c^x)^2}{4(V^{x,xx})^2 + (\omega_c^{xx} - \omega_c^x)^2}, \quad (87)$$

and contains no relaxation parameters. As the strength of the Coulomb coupling increases,  $QE_{<}$  approaches its maximum value of 3/2.

The total QE can be determined from Eqs. (41), (85), and (86) in the limit when time is longer than typical population relaxation time. This results in a sum

$$QE_{>} = \sum_{\bar{\xi}=\pm} \Lambda_{\bar{\xi}}^x \frac{2\Gamma_{xx,\bar{\xi}} + \Gamma_{x,\bar{\xi}}}{\Gamma_{xx,\bar{\xi}} + \Gamma_{x,\bar{\xi}}}, \quad (88)$$

where  $\Lambda_{\bar{\xi}}^x$  determines the probability of optical excitation for each quasiparticle state  $\bar{\xi} = \pm$ , and the ratio of the population relaxation rates gives maximum QE associated with each of the states. (Fig. 8 (b)). As the Coulomb interaction increases,  $QE_{>}$  approaches its maximum value given by the ratio of the *total* population relaxation rates  $(2\Gamma^{xx} + \Gamma^x)/(\Gamma^{xx} + \Gamma^x)$ , where  $\Gamma^x = \Gamma_{x,+} = \Gamma_{x,-}$  and  $\Gamma^{xx} = \Gamma_{xx,+} = \Gamma_{xx,-}$ .<sup>78</sup> Regardless the differences in the relaxation models, similar maximum values for  $QE_{>}$  were obtained in Ref. 46 for increasing Coulomb interaction.

## B. Direct Photogeneration and Impact Ionization Models

Direct Photogeneration Model assumes weak Coulomb coupling between single- and bi-exciton states. Therefore, to find bi-exciton generation rate, we should start with the expressions for photoinduced bi-exciton population (Eq. (71)–(73)) derived in Sec. IV B. Additional assumption of the model is that the pump pulse is much longer than dephasing times resulting in the so called CW limit. This approximation seems to be often the case for the pulse durations used in spectroscopic experiments. The pulse self-convulsion function for quasiparticle populations in CW limit becomes proportional to the Lorentzian line shape function<sup>79</sup>

$$\mathcal{I}_{CW}(\tilde{\omega}_{\bar{\xi}g} - \omega_{pm}) = \frac{2}{\hbar^2} \frac{\mathcal{E}_{pm}^{(0)2} \bar{\tau}_{pm} \gamma_{\bar{\xi}g}}{(\omega_{\bar{\xi}g} - \omega_{pm})^2 + (\gamma_{\bar{\xi}g})^2}, \quad (89)$$

where  $\mathcal{E}_{pm}^{(0)}$  is the pump pulse electric field amplitude, and  $\bar{\tau}_{pm} = \sqrt{\pi}\tau_{pm}$  is effective pulse duration. The pulse self-convulsion function describing the quasiparticle coherences vanishes in CW limit.

Next, we introduce the bi-exciton generation rate as  $W_{xx} = \sum_{k \geq 1} \rho_k^{xx}/\bar{\tau}_{pm}$  where the limit of  $\gamma_{\bar{\xi}0} \rightarrow 0$  should be taken. This according to Eqs. (71) and (73) corresponds to the following expression for the bi-exciton generation rate

$$W_{xx} = \frac{2\pi}{\hbar} \mathcal{E}_{pm}^{(0)2} \sum_{k \geq 1} \sum_{a \geq 1} \left| \Lambda_{k,a}^{xx,x} \mu_{a0}^x \right|^2 \delta(E_a^x - \hbar\omega_{pm}) + \frac{2\pi}{\hbar} \mathcal{E}_{pm}^{(0)2} \sum_{k \geq 1} \left| \sum_{a \geq 1} \Lambda_{k,a}^{xx,x} \mu_{a0}^x + \sum_{l \geq 1} \mu_{kl}^{xx} \bar{\Lambda}_{l,0}^{xx,x} \right|^2 \times \delta(E_k^{xx} - \hbar\omega_{pm}). \quad (90)$$

Here, the interband transition amplitude  $\Lambda_{k,a}^{xx,x}$  is given by Eq. (65), and  $E_a^x = \hbar\omega_a^x$  and  $E_k^{xx} = \hbar\omega_k^{xx}$  are single- and bi-exciton energies, respectively.<sup>80</sup> The leading term to the single exciton generation rate can be easily obtained using the same approach

$$W_x = \frac{2\pi}{\hbar} \mathcal{E}_{pm}^{(0)2} \sum_{a \geq 1} |\mu_{a0}^x|^2 \delta(E_a^x - \hbar\omega_{pm}), \quad (91)$$

and coincides with that given in Ref. 27.

Equation (90) should be compared with Eqs. (1) and (3) describing direct bi-exciton generation rate via virtual single-exciton states and via coupling to the vacuum states derived in Refs. 27 and 47, respectively. The comparison shows that the two contributions to the second term in Eq. (90) multiplied by  $\delta(E_a^x - E_k^{xx})$  and shown in panels (b) and (c) of Fig. 6, reproduce Eqs. (1) and (3) from Refs. 27 and 47, respectively. Eqs. (1) and (3) (Refs. 27, 47 also miss the interference term coming out from Eq. (90). We emphasize that the first term in Eq. (90) describing



the bi-exciton generation rate via direct excitation of single-exciton resonances (Fig. 6 (a)) which is missing in Refs. 27,47 should also be accounted for in the calculations.

Central object of Impact Ionization Model is the impact ionization and Auger recombination rates which can be easily obtained from Eq. (76) by taking the limit of  $\gamma_{a,k}^{x,xx} \rightarrow 0$ , and further performing summation over the final bi- and single-exciton states

$$W_a^{II} = \frac{2\pi}{\hbar} \sum_{k \geq 1} |V_{a,k}^{x,xx}|^2 \delta(E_a^x - E_k^{xx}), \quad (92)$$

$$W_k^{AR} = \frac{2\pi}{\hbar} \sum_{a \geq 1} |V_{a,k}^{x,xx}|^2 \delta(E_a^x - E_k^{xx}), \quad (93)$$

respectively. Comparison of these expressions with Eqs. (1) and (2) from Ref. 49 leads to the conclusion that Impact Ionization Model is just the relaxation component of our model in the weak Coulomb coupling regime (Fig. 7). Usually, the initial condition for the impact ionization dynamics is taken to be only the photogenerated *single*-exciton population (Eq. (67)). We argue that the bi-exciton population described by Eqs. (71)–(73) should also be accounted for, since its contribution can become comparable.

The discussion above shows that Direct Photogeneration Model and Impact Ionization Model complement each other. Specifically, the former one describes the primary photoexcitation event involving pump pulse, which is longer than dephasing time and shorter than the inverse relaxation rates of impact ionization (Eq. (92)), Auger recombination (Eq. (93)) and phonon-assisted decay (Eqs. (77)–(78)). The latter model describes photogenerated population relaxation with the initial conditions given by Eqs. (90)–(91). More systematic approach which we propose here is to follow the weak Coulomb limit computational scheme given in Sec. IV.

### C. Concluding Remarks

Currently, numerical implementation of Exciton Scattering Model is a challenging task, since the calculations will involve a large  $\sim 10^5$  number of bi-exciton states. This poses difficulties on full scattering matrix calculations (Eqs. (24)–(26)) associated with large computer memory requirement for the matrix inversion. The difficulties can be overcome by noticing that in NCs, the energy difference between most of the coupled single- and bi-exciton states is larger than the interband Coulomb interaction, and only small amount of the states is in resonance (degenerate). As a result, the expressions obtained in the weak Coulomb limit (Sec. IV) should be used to evaluate the contributions from well separated states, and only contributions from the degenerate states should be accounted for through multiple-scattering formalism. This demonstrates that Coherent Superposition Model and weak Coulomb limit of the proposed model

are complementary. If the level broadening for the degenerate states in NCs *exceeds* the Coulomb coupling than the computational scheme developed in Sec. IV should be fully used including the degenerate states.

The comparison of CM processes in NCs and in bulk semiconductors is important for understanding the role of quantum-size effects on QE. Therefore, we emphasize that the proposed formalism can be applicable to study CM in bulk semiconductors. The transition is simple: One has to replace all the summations over the single- and bi-exciton indices as well as over the quasiparticle states to the summations over their quasi-momenta and spin degrees of freedom. All matrix elements entering the calculations should be represented in the quasi-momentum basis set. This representation will automatically impose the quasi-momentum conservation restrictions.

To summarize, we have proposed Exciton Scattering Model which treats two main events of CM such as photogeneration and population relaxation on the same footing. The model is valid in the vicinity of AET where the contribution of the higher-multiplicity exciton states (tri-exciton, *etc.*) can be neglected. Proposed model can handle relatively large Coulomb interaction leading to multiple interband scattering events. The only restriction on the Coulomb interaction strength is that it should not mix the higher multiplicity states. Based on general formalism, the expressions determining QE in the limit of weak Coulomb interaction have been derived. This limit is extremely useful for numerical calculations focused on specific materials. As we demonstrated, Exciton Scattering Model recovers all previously proposed models as different limiting cases, and provides a unified approach to study CM in NCs as well as to explore the bulk limit.

### Acknowledgments

This work was supported by the Office of Basic Energy Sciences, US Department of Energy, and Los Alamos LDRD funds. We also acknowledge the support provided by CNLS. We wish to thank Victor I. Klimov, Vladimir Chernyak, Sergei Tretiak, and Darryl L. G. Smith for stimulating discussions and comments on the manuscript.

### APPENDIX A: INTERACTING MULTI-EXCITON HAMILTONIAN

After introducing the electron and hole creation (annihilation) operators  $c_n^\dagger$  ( $c_n$ ) and  $d_m^\dagger$  ( $d_m$ ), respectively, the many-body Hamiltonian describing the valence and conduction band electronic states in semiconductors can be represented as a sum of three components<sup>55</sup>

$$\hat{\mathcal{H}}_{eh} = \hat{\mathcal{H}}_0 + \hat{\mathcal{H}}_1 + \hat{\mathcal{H}}_2. \quad (A1)$$

In this expression, the first term

$$\begin{aligned}\hat{\mathcal{H}}_0 = & \sum_m \epsilon_m^e c_m^\dagger c_m - \sum_n \epsilon_n^h d_n^\dagger d_n \\ & - \sum_{mnlk} (V_{mnlk}^{ehhe} - V_{mnkl}^{ehhe}) c_m^\dagger d_l^\dagger d_n c_k \\ & + \frac{1}{2} \sum_{mnlk} V_{mnlk}^{eeee} c_m^\dagger c_n^\dagger c_l c_k \\ & + \frac{1}{2} \sum_{mnlk} V_{mnlk}^{hhhh} d_l^\dagger d_k^\dagger d_m d_n,\end{aligned}\quad (\text{A2})$$

conserving number of quasiparticles describes non-interacting electrons and holes which are characterized by the Hartree-Fock energies  $\epsilon_n^e$  and  $\epsilon_n^h$ , respectively. Here and below (Eqs. (A2)–(A5)), the superscripts  $e$  and  $h$  denote electrons and holes, respectively, while the corresponding indices run over all Hartree-Fock states in the valence and conduction bands. In Eq. (A2) the Coulomb matrix element is

$$V_{mnlk} = \int d^3x \int d^3y \psi_m^*(x) \psi_n^*(y) V(|x-y|) \psi_l(y) \psi_k(x), \quad (\text{A3})$$

where  $V(|x-y|)$  is the Coulomb potential and  $\psi_n$  is the electron (hole) Hartree-Fock wave function.

The second term in the Hamiltonian (A1)

$$\begin{aligned}\hat{\mathcal{H}}_1 = & \frac{1}{2} \sum_{mnlk} (V_{mnlk}^{ehhe} - V_{mnkl}^{ehhe}) c_m^\dagger d_n c_l c_k \\ & + \frac{1}{2} \sum_{mnlk} (V_{mnlk}^{eehe} - V_{mnkl}^{eehe}) c_m^\dagger c_n^\dagger d_l^\dagger c_k \\ & + \frac{1}{2} \sum_{mnlk} (V_{mnlk}^{hhhe} - V_{mnkl}^{hhhe}) d_l^\dagger d_m d_n c_k \\ & + \frac{1}{2} \sum_{mnlk} (V_{mnlk}^{ehhh} - V_{mnkl}^{ehhh}) c_m^\dagger d_l^\dagger d_k^\dagger d_n\end{aligned}\quad (\text{A4})$$

describes the processes of creation or annihilation of a single electron-hole pair (in the presence of another electron or hole state) which are referred as Auger recombination and impact ionization, respectively. Finally, the last term in the Hamiltonian (A1)

$$\begin{aligned}\hat{\mathcal{H}}_2 = & \frac{1}{2} \sum_{mnlk} V_{mnlk}^{hhee} d_m d_n c_l c_k \\ & + \frac{1}{2} \sum_{mnlk} V_{mnlk}^{eehh} c_m^\dagger c_n^\dagger d_l^\dagger d_k^\dagger\end{aligned}\quad (\text{A5})$$

characterizes the processes which involve simultaneous creation or annihilation of two electron-hole pairs.

Neglecting all possible charged states we consider only the space spanned by all possible multiple electron-hole pairs (multi-excitons)  $S = \oplus_{\bar{n} \geq 0} S^{\bar{n}}$  where  $S^0$  is the exciton vacuum (filled valence band, empty conduction band),  $S^{\bar{n}}$  is an exciton space of multiplicity  $\bar{n}$  with

the complete basis set constructed from non-interacting electron-hole states

$$|e_a^{\bar{n}} h_b^{\bar{n}}\rangle = \Pi_{k=1}^{\bar{n}} c_{a_k}^\dagger d_{b_k}^\dagger |0\rangle, \quad (\text{A6})$$

where the generalized indices are defined as  $\bar{a} = \{a_1, \dots, a_{\bar{n}}\}$  and  $\bar{b} = \{b_1, \dots, b_{\bar{n}}\}$ . In this representation the many-body Hamiltonian term  $\hat{\mathcal{H}}_0$  (Eq. (A2)) maps  $S^{\bar{n}}$  on itself. As a result, one can define the eigenstates  $|X_{\xi}^{\bar{n}}\rangle$  of  $\hat{\mathcal{H}}_0$  forming a complete basis set in  $S^{\bar{n}}$  and, respectively, the eigenenergies  $\hbar\omega_{\xi}^{\bar{n}}$ . The latter eigenstates describe bound  $n$ -exciton states in  $S^{\bar{n}}$  whose eigenenergies include the binding energy due to the electron-electron, hole-hole and electron-hole Coulomb correlations. The introduced bound  $n$ -exciton states are related to the non-interacting electron-hole basis through a unitary transformation

$$|x_{\xi}^{\bar{n}}\rangle = \sum U_{\xi; \bar{a}\bar{b}}^{\bar{n}} |e_a^{\bar{n}} h_b^{\bar{n}}\rangle, \quad (\text{A7})$$

defined by the matrix  $\{U_{\xi; \bar{a}\bar{b}}^{\bar{n}}\}$ .

The eigenstate equations

$$\sum_{pq} \langle h_s e_r | \hat{\mathcal{H}}_0 - \hbar\omega_a^x | e_p h_q \rangle U_{a;pq}^x = 0, \quad (\text{A8})$$

and

$$\sum_{pqrs} \langle h_e e_f h_g e_h | \hat{\mathcal{H}}_0 - \hbar\omega_a^x | e_p h_q e_r h_s \rangle U_{a;pqrs}^{xx} = 0, \quad (\text{A9})$$

determining the transformation matrix elements for the single- and bi-exciton states have the following form

$$\begin{aligned}& \sum_{pq} \{ (\epsilon_p^e - \epsilon_s^h - \hbar\omega_a^x) \delta_{sq} \delta_{rp} \\ & + V_{rqps}^{ehhe} - V_{rqs p}^{ehhe} \} U_{a;pq}^x = 0,\end{aligned}\quad (\text{A10})$$

and

$$\begin{aligned}& \sum_{pqrs} \{ (\delta_{gq} \delta_{es} - \delta_{eq} \delta_{gs}) [(\delta_{hp} \delta_{fr} - \delta_{hr} \delta_{fp}) (\epsilon_h^e + \epsilon_f^e)] \\ & + \frac{1}{2} \sum_{mnlk} (\delta_{fn} \delta_{hm} - \delta_{fm} \delta_{hn}) (\delta_{kp} \delta_{lr} - \delta_{lp} \delta_{kr}) V_{mnlk}^{eeee} \\ & - (\delta_{hp} \delta_{fr} - \delta_{fp} \delta_{hr}) [(\delta_{gs} \delta_{eq} - \delta_{es} \delta_{gq}) (\epsilon_s^h + \epsilon_q^h) \\ & - \frac{1}{2} \sum_{mnlk} (\delta_{nq} \delta_{ms} - \delta_{ns} \delta_{mq}) (\delta_{gl} \delta_{eq} - \delta_{gk} \delta_{el}) V_{mnlk}^{hhhh} \\ & + \sum_{mnlk} [(\delta_{nq} (\delta_{gl} \delta_{es} - \delta_{gs} \delta_{el}) - \delta_{ns} (\delta_{gl} \delta_{eq} - \delta_{gq} \delta_{el})) \\ & \times (\delta_{kp} (\delta_{hm} \delta_{fr} - \delta_{hr} \delta_{fm}) - \delta_{kr} (\delta_{hm} \delta_{fp} - \delta_{hp} \delta_{fm})) \\ & \times (V_{mnkl}^{ehhe} - V_{mnlk}^{ehhe})] \\ & - (\delta_{gq} \delta_{es} - \delta_{eq} \delta_{gs}) (\delta_{hp} \delta_{fr} - \delta_{hr} \delta_{fp}) \hbar\omega_a^{xx} \} U_{a;pqrs}^{xx} = 0,\end{aligned}$$

respectively. Using the transformation matrix defined by the secular equations Eqs. (A10) and (A11) the Coulomb

matrix element entering Eq. (8) becomes

$$V_{a,n}^{x,xx} = \quad (A12)$$

$$\begin{aligned} & \sum_{pq} \sum_{rstv} (U_{a;pq}^x)^* [(V_{pstr}^{chee} - V_{psrt}^{chee}) \delta_{qv} \\ & - (V_{pvtr}^{chee} - V_{pvrt}^{chee}) \delta_{qs}] U_{rstv;n}^{xx} \\ & + \sum_{pq} \sum_{rstv} (U_{a;pq}^x)^* [(V_{vsqr}^{hhhe} - V_{svqr}^{hhhe}) \delta_{pt} \\ & - (V_{svqt}^{hhhe} - V_{vsqt}^{hhhe}) \delta_{pr}] U_{rstv;n}^{xx} \\ V_{0,n}^{0,xx} & = \sum_{rstv} [V_{vsrt}^{hhee} - V_{vstr}^{hhee}] U_{rstv;n}^{xx}. \end{aligned} \quad (A13)$$

## APPENDIX B: THE EXCITON-PHONON INTERACTION HAMILTONIAN

The many-body Hamiltonian accounting for the linear electron-phonon interaction in the electron-hole representation is<sup>55</sup>

$$\begin{aligned} \hat{\mathcal{H}}_{int} &= \sum_{mn\alpha} f_{mn;\alpha}^{ee} q_\alpha c_m^\dagger c_n - \sum_{mn\alpha} f_{mn;\alpha}^{hh} q_\alpha d_m^\dagger d_n \quad (B1) \\ &+ \sum_{nm\alpha} f_{mn;\alpha}^{he} q_\alpha d_m c_n + \sum_{mn\alpha} f_{mn;\alpha}^{eh} q_\alpha c_m^\dagger d_n^\dagger, \end{aligned}$$

where the phonon normal modes are  $\mathbf{q} = \{q_1, \dots, q_\alpha, \dots, q_{N_{ph}}\}$ , and the coupling constants are the following matrix elements

$$f_{mn;\alpha}^{rs} = \langle \psi_m^r | \hat{F}_\alpha | \psi_n^s \rangle, \quad r, s = e, h; \quad (B2)$$

of the force operator  $\hat{F}_\alpha$  averaged over the Hartree-Fock electron and hole wave functions. In this Hamiltonian, we dropped the term  $\sum_{n\alpha} f_{nn;\alpha}^{hh} q_\alpha$ , which has no contribution to the processes under consideration.

Adopting the multi-exciton basis set given by Eq. (A7), the electron-phonon interaction Hamiltonian (B1) can be projected on single- and bi-exciton states resulting in Eq. (33) where the intraband exciton-phonon coupling matrix elements are

$$\begin{aligned} Y_{ab;\alpha}^x &= \sum_{pq=e} \sum_{r=h} U_{a;pr}^x f_{pq;\alpha}^{ee} U_{b;q}^x \quad (B3) \\ &- \sum_{pq=h} \sum_{r=e} U_{a;rp}^x f_{pq;\alpha}^{hh} U_{b;q}^x, \end{aligned}$$

$$\begin{aligned} Y_{mn;\alpha}^{xx} &= \sum_{kgpr=e} \sum_{hfqs=h} U_{m;khgf}^{xx} U_{n;pqrs}^{xx} \quad (B4) \\ &\times (\delta_{hq} \delta_{fs} - \delta_{fq} \delta_{hs}) \\ &\times (\delta_{gr} f_{kp;\alpha}^{ee} - \delta_{gp} f_{kr;\alpha}^{ee} - \delta_{kr} f_{ga;\alpha}^{ee} + \delta_{ka} f_{gr;\alpha}^{ee}) \\ &- \sum_{kgpr=e} \sum_{hfqs=h} U_{m;khgf}^{xx} U_{n;pqrs}^{xx} \\ &\times (\delta_{kp} \delta_{gr} - \delta_{gp} \delta_{kr}) \\ &\times (\delta_{fs} f_{hq;\alpha}^{hh} - \delta_{hs} f_{fq;\alpha}^{hh} - \delta_{fq} f_{hs;\alpha}^{hh} + \delta_{hq} f_{fs;\alpha}^{hh}). \end{aligned}$$

The interband exciton-phonon matrix element also entering Eq. (33) is

$$\begin{aligned} Y_{am;\alpha}^{x,xx} &= \sum_{gpr=e} \sum_{fqs=h} U_{a;gf}^x U_{m;pqrs}^{xx} f_{mn;\alpha}^{he} \quad (B5) \\ &\times (\delta_{fs} \delta_{gr} f_{qp;\alpha}^{he} - \delta_{fs} \delta_{gp} f_{qr;\alpha}^{he} \\ &- \delta_{fq} \delta_{gr} f_{sp;\alpha}^{he} + \delta_{fg} \delta_{gp} f_{sr;\alpha}^{he}). \end{aligned}$$

Here, the transformation matrices  $U^x$  and  $U^{xx}$  can be calculated according to Eqs. (A10) and (A11), respectively.

## APPENDIX C: THE EXCITON-OPTICAL FIELD INTERACTION HAMILTONIAN

The many-body Hamiltonian in the Hartree-Fock orbital representation describing the interaction with time-dependent optical field  $E(t)$  reads<sup>55</sup>

$$\begin{aligned} \hat{\mathcal{H}}_{opt}(t) &= -E(t) \sum_{mn} P_{mn}^{ee} c_m^\dagger c_n \quad (C1) \\ &+ E(t) \sum_{mn} P_{mn}^{hh} d_m^\dagger d_n \\ &- E(t) \sum_{nm} P_{mn}^{he} d_m c_n \\ &- E(t) \sum_{mn} P_{mn}^{eh} c_m^\dagger d_n^\dagger, \end{aligned}$$

where the transition dipole moments are matrix elements

$$P_{mn}^{rs} = \langle \psi_m^r | \hat{\mathbf{e}} \cdot \hat{\mathbf{d}} | \psi_n^s \rangle, \quad r, s = e, h; \quad (C2)$$

of the dipole moment operator  $\hat{\mathbf{d}}$  projected onto the field polarization direction  $\hat{\mathbf{e}}$ , and further averaged over the Hartree-Fock electron and hole wave functions. This Hamiltonian has absolutely the same structure as the electron-phonon coupling Hamiltonian (Eq. (B1)) discussed in Appendix B. Therefore, in direct analogy with Eq. (33), one can immediately recast the former Hamiltonian to the single and bi-exciton state representation given by Eq. (28). The intraband single-exciton (bi-exciton) transition dipoles  $\mu_{ab}^x$  ( $\mu_{mn}^{xx}$ ) entering Eq. (28) can be determined by replacing  $Y_{ab;\alpha}^x$  ( $Y_{nm;\alpha}^{xx}$ ) in the l.h.s. of Eq. (B3) (Eq. (B4)) by  $\mu_{ab}^x$  ( $\mu_{nm}^{xx}$ ). Determination of the interband transition dipoles requires the replacement of  $Y_{am;\alpha}^{x,xx}$  in the l.h.s. of Eq. (B5) by  $\mu_{am}^{x,xx}$ . Also all  $f_{pq;\alpha}^{rs}$  ( $r, s = e, h$ ) in the r.h.s. of Eqs. (B3)–(B5) should be substituted by  $P_{ab}^{rs}$  ( $r, s = e, h$ ).

## APPENDIX D: COHERENT SUPERPOSITION MODEL

Coherent Superposition Model is a limit of Exciton Scattering Model including only two states  $|x_c\rangle$  and  $|xx_c\rangle$

coupled by Coulomb matrix element  $V^{x,xx}$  and two uncoupled states  $|x_u\rangle$  and  $|xx_u\rangle$  characterized by the following Hamiltonian

$$\hat{H} + \sum_{a=c,u} (|x_a\rangle \hbar \omega_a^x \langle x_a| + |xx_a\rangle \hbar \omega_a^{xx} \langle xx_a|) \quad (\text{D1})$$

$$+ |x_c\rangle V^{x,xx} \langle xx_c| + |xx_c\rangle V^{xx,x} \langle x_c|.$$

According to Eqs. (24) and (26) the scattering matrix elements for the coupled states are

$$T_c^x(\omega) = \left( \frac{V^{x,xx}}{\hbar} \right)^2 \frac{(\omega - \omega_c^x)}{i(\omega - \omega_+)(\omega - \omega_-)}, \quad (\text{D2})$$

$$T_c^{xx}(\omega) = \left( \frac{V^{x,xx}}{\hbar} \right)^2 \frac{(\omega - \omega_c^{xx})}{i(\omega - \omega_+)(\omega - \omega_-)}, \quad (\text{D3})$$

$$T_c^{x,xx}(\omega) = \frac{V^{x,xx}}{\hbar} \frac{(\omega - \omega_c^x)(\omega - \omega_c^{xx})}{i(\omega - \omega_+)(\omega - \omega_-)}, \quad (\text{D4})$$

where we denote the eigenenergies (quasiparticle energies) as

$$\omega_{\pm} = \frac{\omega_c^x + \omega_c^{xx}}{2} \pm \sqrt{\left( \frac{\omega_c^x - \omega_c^{xx}}{2} \right)^2 + \left( \frac{V^{x,xx}}{\hbar} \right)^2}. \quad (\text{D5})$$

Following the procedure in Sec. II C, one finds that the corresponding time-dependent Green function components for coupled states are

$$G_c^x(t) = \Lambda_+^x e^{-i\tilde{\omega}_+ t} + \Lambda_-^x e^{-i\tilde{\omega}_- t} \quad (\text{D6})$$

$$1G_c^{xx}(t) = \Lambda_+^{xx} e^{-i\tilde{\omega}_+ t} + \Lambda_-^{xx} e^{-i\tilde{\omega}_- t} \quad (\text{D7})$$

$$G_c^{x,xx}(t) = \Lambda_+^{x,xx} e^{-i\tilde{\omega}_+ t} + \Lambda_-^{x,xx} e^{-i\tilde{\omega}_- t}, \quad (\text{D8})$$

which depend on the transition amplitudes

$$\Lambda_{\pm}^x = \pm \frac{(\omega_{\pm} - \omega_c^{xx})}{(\omega_+ - \omega_-)}, \quad (\text{D9})$$

$$\Lambda_{\pm}^{xx} = \pm \frac{(\omega_{\pm} - \omega_c^x)}{(\omega_+ - \omega_-)}, \quad (\text{D10})$$

$$\Lambda_{\pm}^{x,xx} = \pm \frac{V^{x,xx}}{\hbar(\omega_+ - \omega_-)}. \quad (\text{D11})$$

Note that these quantities are real, since Coulomb coupling significantly exceeds the level broadening.

To find the single- and bi-exciton populations associated with the excitation of the quasiparticle populations, we use the following relaxation equations for populations in the quasiparticle representation (Fig. 8 (b))

$$\dot{\rho}_{\pm} = -(\Gamma_{x,\pm} + \Gamma_{xx,\pm}) \rho_{\pm} \quad (\text{D12})$$

$$\dot{\rho}_u^x = \Gamma_{x,+} \rho_+ + \Gamma_{x,-} \rho_-$$

$$\dot{\rho}_u^{xx} = \Gamma_{xx,+} \rho_+ + \Gamma_{xx,-} \rho_-.$$

The non-vanishing (for  $\tau > 0$ ) components of Liouville space Green function (Eqs. (D12)) are

$$\bar{G}_{\pm;\pm}(\tau) = e^{-(\Gamma_{x,\pm} + \Gamma_{xx,\pm})\tau}, \quad (\text{D13})$$

$$\bar{G}_{u;\pm}^x(\tau) = \frac{\Gamma_{x,\pm}}{\Gamma_{x,\pm} + \Gamma_{xx,\pm}} (1 - \bar{G}_{\pm;\pm}(\tau)),$$

$$\bar{G}_{u;\pm}^{xx}(\tau) = \frac{\Gamma_{xx,\pm}}{\Gamma_{x,\pm} + \Gamma_{xx,\pm}} (1 - \bar{G}_{\pm;\pm}(\tau)).$$

where, the population relaxation rates  $\Gamma_{x,\pm}$  and  $\Gamma_{xx,\pm}$  are given by Eqs. (80) and (81), respectively. For the sake of simplicity, we dropped the population transfer rates between the quasiparticle states.

The time-dependent single and bi-exciton populations due to the excitation of quasiparticle populations are calculated according Eqs. (48) and (50) where Eqs. (D9)–(D11) and (D13) are substituted. For the coupled states these populations are

$$n_c^x(\tau) = \mu^2 \sum_{\xi=\pm} \bar{G}_{\xi,\xi}(\tau) [\Lambda_{\xi}^x]^2 \mathcal{I}(\omega_{\xi} - \omega_{pm}), \quad (\text{D14})$$

$$n_c^{xx}(\tau) = \mu^2 \sum_{\xi=\pm} \bar{G}_{\xi,\xi}(\tau) [\Lambda_{\xi}^{xx}]^2 \mathcal{I}(\omega_{\xi} - \omega_{pm}), \quad (\text{D15})$$

and for the uncoupled states

$$n_u^x(\tau) = \mu^2 \sum_{\xi=\pm} \bar{G}_{u,\xi}^x(\tau) \Lambda_{\xi}^x \mathcal{I}(\omega_{\xi} - \omega_{pm}), \quad (\text{D16})$$

$$n_u^{xx}(\tau) = \mu^2 \sum_{\xi=\pm} \bar{G}_{u,\xi}^{xx}(\tau) \Lambda_{\xi}^{xx} \mathcal{I}(\omega_{\xi} - \omega_{pm}). \quad (\text{D17})$$

Here, the pulse self-convolution function is defined by Eq. (51), and the population Green functions by Eqs. (D13).

The Liouville equation for the coupled state coherence in the quasiparticle basis set reads

$$\dot{\rho}_{+-} = -i\tilde{\omega}_{+-} \rho_{+-}, \quad (\text{D18})$$

where  $\tilde{\omega}_{+-} = \omega_+ - \omega_- - i\gamma_{+-}$  contains  $\omega_{\pm}$  determined by Eq. (D5) and pure dephasing rate  $\gamma_{+-}$  which can be explicitly found by using Eq. (38) and the following quasiparticle-phonon couplings

$$Y_{\pm,\alpha} = Y_{c;\alpha}^x \Lambda_{\pm}^x + 2Y_{cc;\alpha}^{x,xx} \Lambda_{\pm}^{x,xx} + Y_{c;\alpha}^{xx} \Lambda_{\pm}^{xx}, \quad (\text{D19})$$

where  $Y_{c;\alpha}^x$ ,  $Y_{cc;\alpha}^{x,xx}$ ,  $Y_{c;\alpha}^{xx}$  are the component of the coupled exciton states with phonon mode  $\alpha$ .

According to Eq. (47), the contribution of the quasiparticle coherences to the coupled single- and bi-exciton populations are

$$c_c^x(\tau) = 2\mu^2 \Lambda_+^x \Lambda_-^x \text{Re} \{ e^{-i\tilde{\omega}_{+-}\tau} \times \mathcal{I}(\omega_+ - \omega_{pm}; \omega_- - \omega_{pm}) \} \quad (\text{D20})$$

$$c_c^{xx}(\tau) = 2\mu^2 \Lambda_+^{xx} \Lambda_-^{xx} \text{Re} \{ e^{-i\tilde{\omega}_{+-}\tau} \times \mathcal{I}(\omega_+ - \omega_{pm}; \omega_- - \omega_{pm}) \}, \quad (\text{D21})$$

where the pulse self-convolution function is given by Eq. (49). By taking into account that  $\Lambda_+^{xx} \Lambda_-^{xx} = -\Lambda_+^x \Lambda_-^x$ , one finds that  $c_c^x(\tau) = -c_c^{xx}(\tau)$ . Obviously,  $c_u^x(\tau) = c_u^{xx}(\tau) = 0$ .

- \* Electronic address: apiryat@lanl.gov
- <sup>1</sup> S. Kolodinski, J. Werner, T. Wittchen, and H. Queisser, *Appl. Phys. Lett.* **63**, 2405 (1993).
  - <sup>2</sup> A. J. Nozik, *Physica E* **14**, 115 (2002).
  - <sup>3</sup> M. Hanna and A. Nozik, *J. Appl. Phys.* **100**, 074510 (2006).
  - <sup>4</sup> V. Klimov, *Appl. Phys. Lett.* **89**, 123118 (2006).
  - <sup>5</sup> M. C. Beard and R. J. Ellingson, *Laser & Photon. Rev.* **2**, 377 (2008).
  - <sup>6</sup> A. J. Nozik, *Chem. Phys. Lett.* **457**, 3 (2008).
  - <sup>7</sup> J. M. Luther, M. Law, M. C. Beard, Q. Song, M. O. Reese, R. J. Ellingson, and A. J. Nozik, *Nano Lett.* **8**, 3488 (2008).
  - <sup>8</sup> S. Koc, *Czech. J. Phys.* **7**, 91 (1957).
  - <sup>9</sup> A. Smith and D. Dutton, *J. Opt. Soc. Am.* **48**, 1007 (1958).
  - <sup>10</sup> V. Vavilov, *J. Phys. Chem. Solids* **8**, 223 (1959).
  - <sup>11</sup> J. Tauc, *J. Phys. Chem. Solids* **8**, 219 (1959).
  - <sup>12</sup> O. Christensen, *J. Appl. Phys.* **47**, 689 (1976).
  - <sup>13</sup> J. J. H. Pijpers, R. Ulbricht, K. J. Tielrooij, A. Osharov, Y. Golan, C. Delerue, G. Allan, and M. Bonn, *Nature Phys.* (in press).
  - <sup>14</sup> W. Shockley, *Czech. J. Phys.* **11**, 81 (1961).
  - <sup>15</sup> E. Kane, *Phys. Rev.* **159**, 624 (1967).
  - <sup>16</sup> E. Antoncik and N. Gaur, *J. Phys. D: Solid State Phys.* **11**, 735 (1978).
  - <sup>17</sup> M. Wolf, R. Brendel, J. H. Werner, and H. J. Queisser, *J. Appl. Phys.* **83**, 4213 (1998).
  - <sup>18</sup> P. T. Landsberg, *Recombination in Semiconductors* (Cambridge University Press, Cambridge, 1991).
  - <sup>19</sup> D. Harrison, R. A. Abram, and S. Brand, *J. Appl. Phys.* **85**, 8186 (1999).
  - <sup>20</sup> C. A. Klein, *J. Appl. Phys.* **39**, 2029 (1968).
  - <sup>21</sup> R. C. Alig and S. Bloom, *Phys. Rev. Lett.* **35**, 1522 (1975).
  - <sup>22</sup> D. I. Chepic, A. L. Efros, A. I. Ekimov, M. G. Vanov, V. A. Kharchenko, I. A. Kudriavtsev, and T. V. Yazeva, *J. Lumin.* **47**, 113 (1990).
  - <sup>23</sup> A. J. Nozik, *Annu. Rev. Phys. Chem.* **52**, 193 (2001).
  - <sup>24</sup> V. I. Klimov, A. A. Mikhailovsky, S. Xu, A. Malko, J. A. Hollingsworth, C. A. Leatherdale, H. J. Eisler, and M. G. Bawendi, *Science* **290**, 314 (2000).
  - <sup>25</sup> R. D. Schaller and V. I. Klimov, *Phys. Rev. Lett.* **92**, 186601 (2004).
  - <sup>26</sup> R. J. Ellingson, M. C. Beard, J. C. Johnson, P. R. Yu, O. I. Micic, A. J. Nozik, A. Shabaev, and A. L. Efros, *Nano Lett.* **5**, 865 (2005).
  - <sup>27</sup> R. D. Schaller, V. M. Agranovich, and V. I. Klimov, *Nature Phys.* **1**, 189 (2005).
  - <sup>28</sup> R. D. Schaller, M. A. Petruska, and V. I. Klimov, *Appl. Phys. Lett.* **87**, 253102 (2005).
  - <sup>29</sup> R. D. Schaller, M. Sykora, J. M. Pietryga, and V. I. Klimov, *Nano Lett.* **6**, 424 (2006).
  - <sup>30</sup> R. D. Schaller and V. I. Klimov, *Phys. Rev. Lett.* **96**, 097402 (2006).
  - <sup>31</sup> R. D. Schaller, M. Sykora, S. Jeong, and V. I. Klimov, *J. Phys. Chem. B* **110**, 25332 (2006).
  - <sup>32</sup> J. E. Murphy, M. C. Beard, A. G. Norman, S. P. Ahrenkiel, J. C. Johnson, P. R. Yu, O. I. Micic, R. J. Ellingson, and A. J. Nozik, *J. Am. Chem. Soc.* **128**, 3241 (2006).
  - <sup>33</sup> R. D. Schaller, J. M. Pietryga, and V. I. Klimov, *Nano Lett.* **7**, 3469 (2007).
  - <sup>34</sup> M. C. Beard, K. P. Knutsen, P. R. Yu, J. M. Luther, Q. Song, W. K. Metzger, R. J. Ellingson, and A. J. Nozik, *Nano Lett.* **7**, 2506 (2007).
  - <sup>35</sup> J. J. H. Pijpers, E. Hendry, M. T. W. Milder, R. Fanciulli, J. Savolainen, J. L. Herek, D. Vanmaekelbergh, S. Ruhman, D. Mocatta, D. Oron, A. Aharoni, U. Banin, and M. Bonn, *J. Phys. Chem. C* **111**, 4146 (2007).
  - <sup>36</sup> G. Nair and M. G. Bawendi, *Phys. Rev. B* **76**, 081304 (2007).
  - <sup>37</sup> M. Ben-Lulu, D. Mocatta, M. Bonn, U. Banin, S. Ruhman, *Nano Lett.* **8**, 1207 (2008).
  - <sup>38</sup> J. J. H. Pijpers, E. Hendry, M. T. W. Milder, R. Fanciulli, J. Savolainen, and J. L. Herek, D. Vanmaekelbergh, S. Ruhman, D. Mocatta, D. Oron, A. Aharoni, U. Banin, and M. Bonn, *J. Phys. Chem. C* **112**, 4783 (2008).
  - <sup>39</sup> J. A. McGuire, J. Joo, J. M. Pietryga, R. D. Schaller, and V. I. Klimov, *Acc. Chem. Res.* **41**, 1810 (2008).
  - <sup>40</sup> M. T. Trinh, A. J. Houtepen, J. M. Schins, T. Hanrath, J. Piris, W. Knulst, A. P. L. M. Goossens, and L. D. A. Siebbeles, *Nano Lett.* **8**, 1713 (2008).
  - <sup>41</sup> G. Nair, S. M. Geyer, L.-Y. Chang, and M. G. Bawendi, *Phys. Rev. B* **78**, 125325 (2008).
  - <sup>42</sup> M. Ji, S. Park, S. T. Connor, T. Mokari, Y. Cui, and K. J. Gaffney, *Nano Lett.* **9**, 1217 (2009).
  - <sup>43</sup> A. Franceschetti and Y. Zhang, *Phys. Rev. Lett.* **100**, 136805 (2008).
  - <sup>44</sup> M. C. Beard, A. G. Midgett, M. Law, O. E. Semonin, R. J. Ellingson, and A. J. Nozik, *Nano Lett.* **9**, 836 (2009).
  - <sup>45</sup> S. Kilina, S. Ivanov, and S. Tretiak, *J. Am. Chem. Soc.* **131**, 7717 (2009).
  - <sup>46</sup> A. Shabaev, A. L. Efros, and A. J. Nozik, *Nano Lett.* **6**, 2856 (2006).
  - <sup>47</sup> V. I. Rupasov and V. I. Klimov, *Phys. Rev. B* **76**, 125321 (2007).
  - <sup>48</sup> C. M. Isborn, S. V. Kilina, X. Li, and O. V. Prezhdo, *J. Phys. Chem. C* **112**, 1829118294 (2008).
  - <sup>49</sup> A. Franceschetti, J. M. An, and A. Zunger, *Nano Lett.* **6**, 2191 (2006).
  - <sup>50</sup> G. Allan and C. Delerue, *Phys. Rev. B* **73**, 205423 (2006).
  - <sup>51</sup> G. Allan and C. Delerue, *Phys. Rev. B* **77**, 125340 (2008).
  - <sup>52</sup> J.-W. Luo, A. Franceschetti, and A. Zunger, *Nano Lett.* **8**, 3174 (2008).
  - <sup>53</sup> G. Allan and C. Delerue, *Phys. Rev. B* **79**, 195324 (2009).
  - <sup>54</sup> E. Rabani and R. Baer, *Nano Lett.* **8**, 4488 (2008).
  - <sup>55</sup> V. M. Axt and S. Mukamel, *Rev. Mod. Phys.* **70**, 145 (1998).
  - <sup>56</sup> S. Mukamel, *Principles of Nonlinear Optical Spectroscopy* (Oxford University Press, Oxford, 1995).
  - <sup>57</sup> E. N. Economou, *Green's functions in Quantum Physics* (Springer-Verlag, New York, 1983).
  - <sup>58</sup> P. Guyot-Sionnest, B. Wehrenberg, and D. Yu, *J. Chem. Phys.* **123**, 074709 (2005).
  - <sup>59</sup> A. Pandey and P. Guyot-Sionnest, *Science* **322**, 929 (2008).
  - <sup>60</sup> S. V. Kilina, C. F. Craig, D. S. Kilin, and O. V. Prezhdo, *J. Phys. Chem. C* **111**, 4871 (2007).
  - <sup>61</sup> S. V. Kilina, D. S. Kilin, and O. V. Prezhdo, *ACS Nano* **3**, 93 (2009).
  - <sup>62</sup> R. Kubo, M. Toda, and N. Hashitsume, *Statistical Physics II*, No. 31 in *Solid-state sciences*, 2nd ed. (Springer, Berlin, 1995).
  - <sup>63</sup> N. G. van Kampen, *Stochastic Processes in Physics and Chemistry* (North-Holland, Amsterdam, 1992).
  - <sup>64</sup> M. Dahlbom, T. Minami, V. Chernyak, T. Pullerits, V.

- Sundstrom, and S. Mukamel, J. Phys. Chem. B **104**, 3976 (2000).
- <sup>65</sup> R. R. Ernst, G. Bodenhausen, and A. Wokaun, *Principles of Nuclear Magnetic Resonance in One and Two Dimensions* (Clarendon Press, Oxford, 1990).
- <sup>66</sup> R. Zwanzig, *Nonequilibrium Statistical Mechanics* (Oxford University Press, New York, 2001).
- <sup>67</sup> H. Kamisaka, S. V. Kilina, K. Yamashita, and O. V. Prezhdo, Nano Lett. **6**, 2295 (2006).
- <sup>68</sup> H. Kamisaka, S. V. Kilina, Y. Y., and O. V. Prezhdo, J. Phys. Chem. C **112**, 7800 (2008).
- <sup>69</sup> The pump envelope and spatial phases do not contribute to the population dynamics and therefore are dropped.
- <sup>70</sup> Using this representation for the transition amplitude, Eqs. (40) and (39) can be derived by straight forward transformation between the exciton and quasiparticle basis sets using the following relationship  $\langle l|\xi\rangle\langle\xi|r\rangle = \bar{\Lambda}_{lr}(\omega_{\bar{\xi}})$  discussed in Ref. 57
- <sup>71</sup> Eqs. (43)–(45) are obtained in the second order perturbation theory where the small parameter is  $V_{0,k}^{x,x}/E_g$ . We also used the fact that in semiconductor NCs  $E_g \gg k_B T$ .
- <sup>72</sup> The poles are assumed to be of the first order which is a general situation for arbitrary Coulomb coupling. Two poles can coincide if we use the second order expansion of Eq. (21). This results in the renormalization of the energy in the exponential but the form of Eq. (45) will still be the same.
- <sup>73</sup> Deriving Eqs. (47) and (48), we used the following relationship between the components of the equilibrium density matrix and transition amplitude  $\Lambda_{lr}(\omega_0) = \bar{\rho}_{lr}$ .
- <sup>74</sup> Note that in Eq. (50) for  $n_s(0)$ , the population Green function becomes  $\bar{\mathcal{G}}_{\bar{\zeta},\bar{\xi}}(0) = \delta_{\bar{\zeta},\bar{\xi}}$ , and associated prefactor simplifies to  $\sum_{\bar{\zeta}} [\bar{\Lambda}_{ss}(\omega_{\bar{\zeta}})\bar{\mathcal{G}}_{\bar{\zeta},\bar{\xi}}(0)\bar{\Lambda}_{lr}(\omega_{\bar{\xi}})] = \delta_{sl}\delta_{sr}$ .
- <sup>75</sup> Formally, the expression for the interband population transfer rate  $\Gamma_{ak}^{x,xx} = \hbar^{-2} \sum_{\alpha\alpha'} Y_{ak;\alpha}^{x,xx} Y_{ka;\alpha'}^{xx,x} C_{\alpha\alpha'}(\omega_a^x - \omega_k^{xx})$  can be introduced. However, in this expression  $Y_{ka;\alpha'}^{xx,x} \neq 0$  only for the states which have  $\hbar(\omega_k^{xx} - \omega_a^x) > E_g$ . Since  $E_g$  significantly exceeds the phonon bath spectral widths  $\Gamma_{ak}^{x,xx} = 0$ .
- <sup>76</sup> This follows from the observation that for  $V^{x,xx} \rightarrow 0$ ,  $\Lambda_+^x = \Lambda_-^{xx} = 1$  and  $\Lambda_-^x = \Lambda_+^{xx} = 0$ .
- <sup>77</sup> It is easy to show that for small  $\tau_{pm}$  the Gaussian pulse envelope can be approximated as  $\mathcal{E}_{pm}(t) = \mathcal{E}_{pm}^{(0)} e^{-t^2/2\tau_{pm}^2} \approx \sqrt{2\pi\tau} \mathcal{E}_{pm}^{(0)} \delta(t)$  and further substituted into Eqs. (49) and (51) to get the pulse self-convolution functions.
- <sup>78</sup> The equalities require that  $C_\alpha(\omega)$  is a constant for  $\omega$  varying within the range defined by  $V^{x,xx}$ .
- <sup>79</sup> This expression can be rigorously derived by using the Gaussian form for the envelope function  $\mathcal{E}_{pm}(t) = \mathcal{E}_{pm}^{(0)} e^{-t^2/2\tau_{pm}^2}$ . Another way to get Eq. (89) for generic pulse envelope is to assume that  $\mathcal{E}_{pm}^{(0)} = \text{const}$  in the coherence integral over  $t_1$ , and that the pulse auto-correlation function  $\int_{-\infty}^{\infty} dt' \mathcal{E}_{pm}(t') \mathcal{E}_{pm}(t' - t_1) \sim \tau_{pm} \mathcal{E}_{pm}^{(0)2}$ .
- <sup>80</sup> The self-energy contribution to the energy is dropped because they correspond to the fourth order corrections.